



# **The Effect of End Conditions on the Axisymmetric Vibrations of Cylindrical Shells**

**D.P. Adler**

**August 1993**

**UWFDM-921**

M.S. thesis.

***FUSION TECHNOLOGY INSTITUTE***  
***UNIVERSITY OF WISCONSIN***  
***MADISON WISCONSIN***

### **DISCLAIMER**

This report was prepared as an account of work sponsored by an agency of the United States Government. Neither the United States Government, nor any agency thereof, nor any of their employees, makes any warranty, express or implied, or assumes any legal liability or responsibility for the accuracy, completeness, or usefulness of any information, apparatus, product, or process disclosed, or represents that its use would not infringe privately owned rights. Reference herein to any specific commercial product, process, or service by trade name, trademark, manufacturer, or otherwise, does not necessarily constitute or imply its endorsement, recommendation, or favoring by the United States Government or any agency thereof. The views and opinions of authors expressed herein do not necessarily state or reflect those of the United States Government or any agency thereof.

**The Effect of End Conditions on the  
Axisymmetric Vibrations of Cylindrical Shells**

D.P. Adler

Fusion Technology Institute  
University of Wisconsin  
1500 Engineering Drive  
Madison, WI 53706

<http://fti.neep.wisc.edu>

August 1993

UWFDM-921

M.S. thesis.

THE EFFECT OF END CONDITIONS ON  
THE AXISYMMETRIC VIBRATIONS OF CYLINDRICAL SHELLS

by

DOUGLAS PETER ADLER

A thesis submitted in partial fulfillment of  
the requirements for the degree of

MASTER OF SCIENCE  
*Mechanical Engineering*

at the  
UNIVERSITY OF WISCONSIN-MADISON  
1993

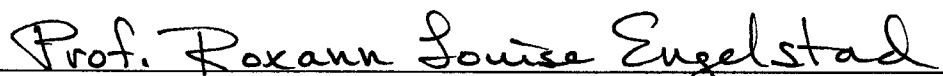
THE EFFECT OF END CONDITIONS ON  
THE AXISYMMETRIC VIBRATIONS OF CYLINDRICAL SHELLS

Douglas Peter Adler

Under the Supervision of Professor Roxann Louise Engelstad

The axisymmetric vibration characteristics of cylinders must be known in order to predict the response to uniform internal blast loads. The closed-form analytical solutions defining cylinder vibrations are very complicated, so numerical methods were employed. The finite element method was used to develop a model for predicting the natural frequencies and the corresponding mode shapes. This model was also used to determine the effect of various cylinder dimensions and end conditions. Unusual "superimposed" mode shapes were found to occur under axial restraint or when sufficient mass was applied to the ends of the cylinder. An experimental investigation was carried out to benchmark the finite element models and verify the existence of the superimposed modes.

Approved:



Professor Roxann Louise Engelstad  
Mechanical Engineering

## ACKNOWLEDGMENT

I would like to thank my advisor Professor Roxann Engelstad for her help and guidance throughout the course of this research. I would also like to thank Professor Edward Lovell for his insight and advice on structural vibrations. I am grateful to Professor Gerald Kulcinski and the rest of the Fusion Technology Institute staff for their continued support of target chamber structural analysis activities.

Funding for this research was provided by the U.S. Department of Energy and Sandia National Laboratories, through the Fusion Technology Institute. The Engineering Mechanics and Astronautics Department made available facilities and equipment for the experimental modal analysis.

## TABLE OF CONTENTS

	PAGE
ABSTRACT .....	ii
ACKNOWLEDGMENT .....	iii
LIST OF FIGURES .....	vi
LIST OF TABLES .....	viii
LIST OF SYMBOLS .....	ix
CHAPTER 1 .....	1
INTRODUCTION .....	1
1.1 Inertial Confinement Fusion Application .....	1
1.2 Thesis Overview .....	3
1.3 References .....	3
CHAPTER 2 .....	4
LITERATURE REVIEW .....	4
2.1 Previous Cylindrical Target Chamber Analyses .....	4
2.2 Cylinder Response to Transient Axisymmetric Loads .....	5
2.3 General Cylinder Vibrations .....	6
2.4 References .....	8
CHAPTER 3 .....	11
ANALYTICAL VIBRATION CHARACTERISTICS .....	11
3.1 Equations of Motion .....	11
3.2 General Cylinder Vibrations .....	14
3.3 Axisymmetric Cylinder Vibrations .....	17
3.4 Effect of Neglecting Longitudinal Inertia .....	19
3.5 Effect of End Conditions .....	22
3.6 References .....	24
CHAPTER 4 .....	26
FINITE ELEMENT MODAL ANALYSIS .....	26
4.1 Modeling .....	26
4.2 General Cylinder Vibrations .....	27
4.3 Axisymmetric Cylinder Vibrations .....	32
4.4 Effect of Cylinder Dimensions .....	35
4.5 Effect of End Conditions .....	41

4.6	References.....	47
CHAPTER 5	.....	51
EXPERIMENTAL MODAL ANALYSIS	.....	51
5.1	Experimental Setup.....	51
5.2	Experimental Procedure.....	54
5.3	Experimental Results for Free Conditions.....	57
5.4	Experimental Results with End Plates .....	59
5.5	References.....	61
CHAPTER 6	.....	62
SUMMARY AND CONCLUSIONS	.....	62



## LIST OF FIGURES

	PAGE
Fig. 3.1 Cylindrical coordinate system and displacement components .....	11
Fig. 3.2 Mode shapes of simply supported cylinders.....	15
Fig. 3.3 Frequency spectrum for simply supported cylinders.....	16
Fig. 3.4 Frequency spectrum for $n=0$ with longitudinal inertia neglected.....	19
Fig. 3.5 Frequency spectrum for $n=0$ , with and without longitudinal inertia .....	21
Fig. 3.6 Effect of end conditions on the frequency spectrum for $n=0$ .....	23
Fig. 3.7 Mode shape and force distributions for lowest axisymmetric mode .....	23
Fig. 4.1 Half cylinder finite element model .....	28
Fig. 4.2 Deformed mesh plot showing the mode shape $m=1$ and $n=6$ .....	30
Fig. 4.3 Contour plot of radial displacements for the $m=1$ and $n=6$ mode shape .....	31
Fig. 4.4 Deformed mesh plot of lowest axisymmetric mode from half cylinder model ( $m=1, n=0$ ) .....	33
Fig. 4.5 Comparison of finite element and analytical results for lowest axisymmetric mode.....	34
Fig. 4.6 Mode shapes with $l/a=4, a/h=20$ (simply supported end conditions).....	36
Fig. 4.7 Mode shapes with $l/a=2, a/h=20$ (simply supported end conditions).....	38
Fig. 4.8 Mode shapes with $l/a=4, a/h=100$ (simply supported end conditions)....	39
Fig. 4.9 Frequency spectrum for $n=0$ from finite element models (simply supported end conditions).....	40
Fig. 4.10 Mode shapes with $l/a=4, a/h=20$ (free end conditions) .....	42
Fig. 4.11 Mode shapes with $l/a=4, a/h=20$ (end conditions $u=w=0$ ) .....	43
Fig. 4.12 Mode shapes with $l/a=4, a/h=20$ (end conditions $u=w=\partial w/\partial x=0$ ) .....	46
Fig. 4.13 Mode shapes with $l/a=2, a/h=20$ (end conditions $u=w=0$ ) .....	48

Fig. 4.14	Mode shapes with $l/a=8$ , $a/h=20$ (end conditions $u=w=0$ ) .....	49
Fig. 4.15	Effect of axial restraint on frequency spectrum.....	50
Fig. 5.1	Schematic of experimental modal analysis setup .....	53
Fig. 5.2	Photo of experimental modal analysis setup .....	53
Fig. 5.3	Representation of experimental measurements and corresponding mode plot .....	56
Fig. 5.4	Mode shapes with free end conditions, showing experimental and finite element results .....	58
Fig. 5.5	Mode shapes with end plates, showing experimental and finite element results .....	60

## LIST OF TABLES

	PAGE
Table 4.1 Comparison of finite element and analytical modal frequencies .....	29
Table 5.1 List of experimental equipment .....	52
Table 5.2 Comparison of experimental and finite element results with free end conditions ( $n=0$ ) .....	57
Table 5.3 Comparison of experimental and finite element results with clamped end conditions simulated by end plates ( $n=0$ ) .....	59

## LIST OF SYMBOLS

$a$	shell radius
$E$	elastic modulus of material
$h$	shell thickness
$l$	shell length
$r$	radial direction
$t$	time
$u$	axial displacement
$v$	circumferential displacement
$w$	radial displacement
$x$	axial direction
$\theta$	circumferential direction
$\rho$	material density
$\nu$	Poisson's ratio

## **Chapter 1**

### **Introduction**

The vibration characteristics of cylindrical shells have been of great interest for many years due to their wide range of applications. Hundreds of papers have been written on the subject, with the earliest dating to the late 1880's. The majority of these papers have dealt with a few select sets of boundary conditions. In many design applications, the vibration characteristics of machines and components are of interest primarily for removing unwanted noise or harmful resonances. This type of work is often done after the initial design has been completed. However, in some applications the structural dynamics play a crucial role in the initial design, and therefore must be thoroughly understood.

#### **1.1 Inertial Confinement Fusion Application**

Inertial Confinement Fusion (ICF) reaction chambers provide a unique application of cylindrical shells which demands a thorough knowledge of their vibration characteristics. In ICF, small fuel pellets (typically composed of deuterium and tritium inside a spherical shell) are exposed to a sudden blast of energy in the form of highly energized particles from lasers, ion beams, or x-rays. The energy from the beams is transferred into kinetic energy as the spherical shell implodes. When the imploding material arrives in the center, it is highly compressed and heated. When the fuel reaches a temperature of 50,000,000 C° and a density 1000 times solid density, the deuterium and tritium fuse to form helium. This reaction releases a huge amount of energy in the form of a small explosion of neutrons, x-rays, and ions over a time period of only a few nanoseconds [1.1]. These particles

create what amounts to a large pressure blast load on the inside of the target chamber.

When a structure is loaded impulsively, it absorbs the energy from the impulse and dissipates it by vibrating at its natural frequencies. The stresses in the structure are often higher during the resulting free vibration than immediately following the impulse. An additional complication results from the rapid heating of the gases within the chamber, which produces a longer duration transient pressure load starting soon after the initial blast. As a result, the vibration characteristics of the chamber are of critical importance in determining a feasible design. The purpose of this research was to develop finite element models to simulate the dynamic response of cylindrical chambers to these blast loadings. Once the finite element models were verified, they could be used to determine the chamber parameters (such as diameter, length, thickness, etc.) required to withstand a particular loading. Thus, the actual chamber design could be developed via the numerical simulations.

Analytical solutions to the problem of cylinder vibrations were sought from the literature in order to verify the finite element models. Because the pressure blast is nearly uniform on the inside of the cylinder, the resulting vibrations will be primarily axisymmetric, or the same all the way around the circumference. During the course of the research it was found that the existing literature was somewhat lacking in the area of axisymmetric cylinder vibrations. Some discrepancies between popular solution methods were found, and unusual mode shapes that had not been previously published have now been identified.

## 1.2 Thesis Overview

In this thesis, Chapter 2 is a general review of the literature on cylinder vibrations. Chapter 3 gives a more in-depth look at the previous work as applied to the current case, and points out some of the difficulties in finding analytical solutions. The modes of vibration are described, and the limitations of various shell theories are discussed.

The finite element modeling is discussed in Chapter 4. The effect of various end conditions is investigated, and the results are compared to the analytical solutions of the previous chapter. Unusual behavior in the form of distinctive "superimposed" mode shapes is presented, and the influence of shell dimensions and supports on these mode shapes is discussed. An attempt is made to generalize this behavior. An experimental investigation was undertaken to verify the modes, the results of which are presented in Chapter 5. Summary and conclusions are given in Chapter 6.

## 1.3 References

- [1.1] Duderstadt, J. J. and Moses, G. A., *Inertial Confinement Fusion*, Wiley, New York, NY, 1982.

## **Chapter 2**

### **Literature Review**

The vibratory response of shells to internal blast loading is of critical importance in the mechanical design of ICF reaction chambers. Spherical shells are usually used for containing explosions, so research on the use of cylindrical shells for this purpose is somewhat limited. Because the internal loading is primarily axisymmetric, the cylinder will respond in a similar fashion. Thus, in this case the axisymmetric vibrations of cylindrical shells are of interest.

#### **2.1 Previous Cylindrical Target Chamber Analyses**

Reaction chambers for ICF applications must contain the blasts from small thermonuclear explosions. A spherical shell is usually desired for containing explosions as they are the most efficient structurally. However, the benefits of cylindrical shells for other design considerations (e.g., manufacturability, ease of access, maintenance, etc.) have led researchers to investigate the use of cylindrical chambers to contain the explosions.

In the HYLIFE reactor study, a waterfall of liquid lithium protects the chamber wall from the explosion [2.1]. Some of the lithium is driven into the wall, producing a pressure pulse lower in magnitude and much longer in duration than the original explosion. In this analysis, the response of the cylinder is roughly approximated by applying a dynamic loading factor to the hoop stress of the cylinder.

In support of the Target Development Facility (TDF) design study, Engelstad and Lovell [2.2] determined the dynamic response of a cylindrical chamber to perform



lifetime calculations. The mechanical response was based on Donnell's equations of motion. The solution was obtained by assuming displacements in the form of a series of combined trigonometric and hyperbolic functions. A frequency equation yielded the natural frequencies, which were then used to determine the mode shapes. The dynamic response to a uniform impulse was calculated using modal superposition. These results were then used to determine the fatigue life of the chamber under repeated blasts.

This work was refined in studies of the Laboratory Microfusion Facility (LMF) by Engelstad, Lovell, and Powers [2.3, 2.4]. ICF target chambers often require a large number of perforations for the ignition beams to pass through. The effect of these perforations was taken into account using modified material properties as developed for fission reactor tube sheet design. The equations developed previously by Lovell were then used to predict the response. More complex load histories composed of impulse, step, and ramped-step functions were also considered to account for a dynamic afterpressure following the initial explosion. The resulting stress histories were again used in fatigue calculations to determine the feasibility of proposed chamber designs.

## **2.2 Cylinder Response to Transient Axisymmetric Loads**

Apart from the ICF work listed above, only two references were found that dealt specifically with the response of cylindrical shells to transient axisymmetric loading. The first is a paper by Wang et al. [2.5] that provides a solution similar to those listed above [2.2-2.4]. Although it precedes these works by 20 years, they were carried out independently. The second by Sheng [2.6] breaks the transient response into two

parts: a static portion and a normal mode portion. However, the method used is computationally intensive and the author gives no examples of the resulting mode shapes. It also appears that the method is tailored for loadings that have a relatively long application period, and limitations on the loading period are not mentioned.

### 2.3 General Cylinder Vibrations

Many investigators (Love, Flügge, Timoshenko, and others) have developed the differential equations of motion which describe the behavior of thin shells. Some of these fundamental works date back to the 1880's. These formulations are well known and published in many texts, so the literature review here will concentrate on more recent works applicable to the current situation.

Many of the early authors derived the equations of motion for general cylinder vibrations, but considered the equations too difficult to solve. Flügge [2.7] developed a similar set of the general equations of motion. He was able to determine the frequency equations for cylinders with simply supported ends by assuming a trigonometric displacement solution. The roots of this equation gave three different natural frequencies for every nodal pattern, each of which corresponded to different amplitude ratios of displacements in the three coordinate directions. Fortunately, the two sets of higher frequencies were typically an order of magnitude above the lowest. He also outlined the solution method for other support conditions, but the method involved the repeated numerical evaluation of an eighth-order determinant, which was not practical until digital computers came of age.

Arnold and Warburton used energy methods to derive the equations of motion and solved them for simply supported [2.8] and clamped [2.9] boundary conditions.

They identified an unusual behavior of cylinders, in that the ordering of the natural frequencies does not always correspond to the complexity of the nodal pattern. They also presented experimental results to verify their analytical work.

Yu [2.10] simplified the Donnell equations for the case where the axial wavelength was very large compared to the circumferential wavelength. He obtained the frequency equations for clamped, simply supported, and mixed end conditions.

The solution method introduced by Flügge for general cylinder vibrations was carried out by Forsberg using digital computers, and his results were presented in three parts. In Ref. [2.11] he considered the effect of various boundary conditions on the flexural vibration characteristics, including frequency, mode shape, and modal stresses. The effect of various assumptions on the solution was considered in Ref. [2.12]. In this paper he considered flexural, beam-type, and axisymmetric vibrations. The effect of end conditions on beam-type and axisymmetric vibrations were covered in Ref. [2.13].

Working independently of Forsberg, Ludwig and Kreig [2.14] used the same solution method and obtained similar results for the mode shapes and frequencies. They considered various mixed end conditions, including numerical results only for shells with a rigid flange at one or both ends. In spite of the different end conditions, many of the mode shapes displayed characteristics similar to those noted by Forsberg.

Smith and Haft [2.15] extended Forsberg's first work to beam-type vibrations. In Ref. [2.16], Vronay and Smith improved upon Forsberg's solution method by making it less tedious. The method is still far from easy and requires excessive

computations. However, it still provides the most exact solution of the equations of motion.

An extensive publication by Liessa [2.17] is a compilation of a wealth of information about shell vibrations. A large portion considers cylindrical shells, and compares results from a large number of researchers including many of the works mentioned here. He showed that most of the various formulations of the general equations of motion (Love, Flügge, Timoshenko, and others) are very similar and yield the same numerical results within engineering accuracy.

A brief note by Goldman [2.18] clarifies the results from Forsberg for the lowest axisymmetric mode shape of a clamped cylinder, and points out that misconceptions about this case may arise from available literature.

This thesis attempts to resolve these misconceptions. Also, results are presented for unusual superimposed mode shapes which differ in appearance from what is normally expected. The exact solution of the equations of motion used by several authors as noted above is extremely laborious, so results are presented which substantiate the use of finite element methods for cylinder vibration analysis.

## 2.4 References

- [2.1] Pitts, J., "A Consistent HYLIFE Wall Design that Withstands Transient Loading Conditions," *Proceedings of the Fourth Topical Meeting on the Technology of Controlled Fusion*, 1980, pp. 1174-1181.
- [2.2] Engelstad, R. L. and Lovell, E. G., "Parametric Lifetime Analysis of Cylindrical Chambers for the Target Development Facility," University of Wisconsin Fusion Technology Report UWFD-656, October 1985.

- [2.3] Engelstad, R. L., Powers, J. P., and Lovell, E. G., "Mechanical Design of the LMF Target Chamber," University of Wisconsin Fusion Technology Report UWFD-656, October 1985.
- [2.4] Powers, J. P., "Structural and Fatigue Analysis of the Sandia Laboratory Microfusion Reaction Chamber," M.S. thesis, 1991, University of Wisconsin-Madison, Madison, WI.
- [2.5] Wang, J. T., Stadler, W., and Lin, C., "The Axisymmetric Response of Cylindrical and Hemispherical Shells to Time-Dependent Loading," NASA CR-572, 1966.
- [2.6] Sheng, J., "The Response of a Thin Cylindrical Shell to Transient Surface Loading," *American Institute of Aeronautics and Astronautics Journal*, Vol. 3, No. 4, April 1965, pp. 701-709.
- [2.7] Flügge, W., *Stresses in Shells*, Springer-Verlag, Berlin, 1960, Chap. 5, pp. 219-233.
- [2.8] Arnold, R. N. and Warburton, G. B., "Flexural Vibrations of the Walls of Thin Cylindrical Shells Having Freely Supported Ends," *Proceedings of the Royal Society (London)*, A, Vol. 197, 1949, p. 238-256.
- [2.9] Arnold, R. N. and Warburton, G. B., "Flexural Vibrations of Thin Cylinders," *Proceedings of the Institution of Mechanical Engineers (London)*, Vol. 167, 1953, pp. 62-80.
- [2.10] Yu, Y. Y., "Free Vibrations of Thin Cylindrical Shells Having Finite Length with Freely Supported and Clamped Ends," *Journal of Applied Mechanics*, Vol. 23, 1955, pp. 547-552.
- [2.11] Forsberg, K., "Influence of Boundary Conditions on the Modal Characteristics of Cylindrical Shells," *American Institute of Aeronautics and Astronautics Journal*, Vol. 2, No. 12, Dec. 1964, pp. 2150-2167.
- [2.12] Forsberg, K., "A Review of Analytical Methods Used to Determine the Modal Characteristics of Cylindrical Shells," NASA CR-613, 1965.
- [2.13] Forsberg, K., "Axisymmetric and Beam-Type Vibrations of Thin Cylindrical Shells," *American Institute of Aeronautics and Astronautics Journal*, Vol. 7, No. 2, Feb. 1969, pp. 221-227.
- [2.14] Ludwig, A. and Krieg, R., "An Analytical Quasi-exact Method for Calculating Eigenvibrations of Thin Circular Cylindrical Shells," *Journal of Sound and Vibration*, Vol. 74, No. 2, 1981, pp. 155-174.
- [2.15] Smith, B. L. and Haft, E. E., "Natural Frequencies of Clamped Cylindrical Shells," *American Institute of Aeronautics and Astronautics Journal*, Vol. 6, No. 4, April 1968, pp. 720-721.

- [2.16] Vronay, D. F. and Smith, B. L., "Free Vibrations of Circular Cylindrical Shells of Finite Length" *American Institute of Aeronautics and Astronautics Journal*, Vol. 8, No. 3, March 1970, pp. 601-603.
- [2.17] Leissa, A. W., *Vibration of Shells*, NASA SP-288, 1973.
- [2.18] Goldman, R. L., "Mode Shapes and Frequencies of Clamped-Clamped Cylindrical Shells," *American Institute of Aeronautics and Astronautics Journal*, Vol. 12, No. 12, Dec. 1974, pp. 1755-1756.

## Chapter 3

### Analytical Vibration Characteristics

The analytical solution of cylinder vibrations is extremely difficult and computationally intensive. In this chapter, results from various authors are compiled and compared to provide an introduction to the characteristics of vibrating cylinders.

#### 3.1 Equations of Motion

The present research is limited to circular cylindrical shells, so the cylindrical coordinate system shown in Fig. 3.1 is used to define the equations of motion. The axial, circumferential, and radial directions are denoted (respectively) by  $x$ ,  $\theta$ , and  $r$ , and the corresponding displacements are  $u$ ,  $v$ , and  $w$ . The shell dimensions are given by the following:  $h$  is the thickness,  $a$  is the radius, and  $l$  is the length.

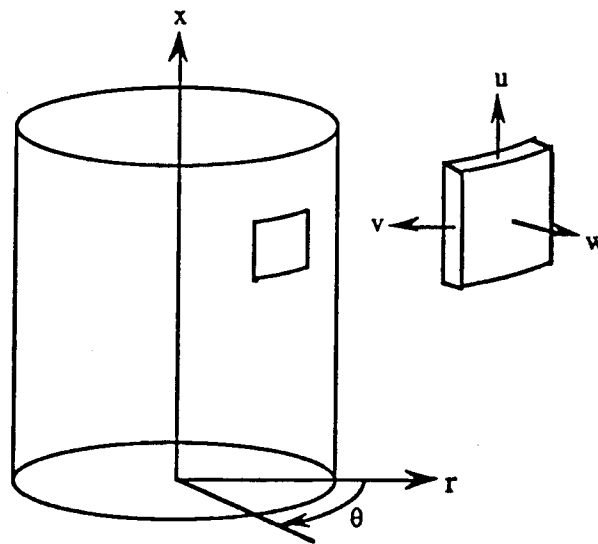


Fig. 3.1. Cylindrical coordinate system and displacement components.

This analysis follows the common assumptions of linear thin shell theory, i.e., the cylinder is assumed to be thin ( $a/h > 10$ ), of constant wall thickness, and made of a linear, isotropic, homogeneous material. As previously mentioned, there are many different formulations of the general differential equations of motion for thin shell vibrations (Love, Flügge, Timoshenko, and others). If the thin shell criterion is met, then most of the formulations of the general equations of motion give similar results [3.1, 3.2]. The equations as developed by Flügge [3.3] are:

$$\frac{\partial^2 u}{\partial x^2} + \frac{1-\nu}{2}(1+k) \frac{\partial^2 u}{\partial \theta^2} + \frac{1+\nu}{2} \frac{\partial^2 v}{\partial x \partial \theta} - k \frac{\partial^3 w}{\partial x^3} + \frac{1-\nu}{2} k \frac{\partial^3 w}{\partial x \partial \theta^2} + \nu \frac{\partial w}{\partial x} - \gamma^2 \frac{\partial^2 u}{\partial t^2} = 0 \quad (3.1a)$$

$$\frac{1+\nu}{2} \frac{\partial^2 u}{\partial x \partial \theta} + \frac{\partial^2 v}{\partial \theta^2} + \frac{1-\nu}{2}(1+3k) \frac{\partial^2 v}{\partial x^2} - \frac{3-\nu}{2} k \frac{\partial^3 w}{\partial x^2 \partial \theta} + \frac{\partial w}{\partial \theta} - \gamma^2 \frac{\partial^2 v}{\partial t^2} = 0 \quad (3.1b)$$

$$\begin{aligned} -k \frac{\partial^3 u}{\partial x^3} + \frac{1-\nu}{2} k \frac{\partial^3 u}{\partial x \partial \theta^2} + \nu \frac{\partial u}{\partial x} - \frac{3-\nu}{2} k \frac{\partial^3 v}{\partial x^2 \partial \theta} + \frac{\partial v}{\partial \theta} + (1+k)w \\ + 2k \frac{\partial^2 w}{\partial \theta^2} + k \nabla^4 w + \gamma^2 \frac{\partial^2 w}{\partial t^2} = 0 \end{aligned} \quad (3.1c)$$

where

$$\gamma^2 = \frac{\rho a^2 (1-\nu^2)}{E} \quad (3.1d)$$

$$k = \frac{h^2}{12a^2} \quad (3.1e)$$

$$\nabla^2 = \frac{\partial^2}{\partial x^2} + \frac{\partial^2}{\partial \theta^2} \quad (3.1f)$$



and  $E$  is the elastic modulus of the material,  $\rho$  is the density,  $\nu$  is Poisson's ratio, and  $t$  denotes time. Note that the axial coordinate  $x$  has been nondimensionalized by dividing by the radius.

The complexity of the above equations helps explain why so many different formulations exist. Many of the terms involve the strain-displacement relationships and other aspects with little effect on the vibration characteristics. Researchers have attempted various simplifications in order to solve these equations. Donnell [3.4] showed that if the radius to thickness ratio is assumed negligible compared to unity, considerable simplification of the equations results, e.g.,

$$\frac{\partial^2 u}{\partial x^2} + \frac{1-\nu}{2} \frac{\partial^2 u}{\partial \theta^2} + \frac{1+\nu}{2} \frac{\partial^2 v}{\partial x \partial \theta} + \nu \frac{\partial w}{\partial x} - \gamma^2 \frac{\partial^2 u}{\partial t^2} = 0 \quad (3.2a)$$

$$\frac{1+\nu}{2} \frac{\partial^2 u}{\partial x \partial \theta} + \frac{\partial^2 v}{\partial \theta^2} + \frac{1-\nu}{2} \frac{\partial^2 v}{\partial x^2} + \frac{\partial w}{\partial \theta} - \gamma^2 \frac{\partial^2 v}{\partial t^2} = 0 \quad (3.2b)$$

$$\nu \frac{\partial u}{\partial x} + \frac{\partial v}{\partial \theta} + w + k \nabla^4 w + \gamma^2 \frac{\partial^2 w}{\partial t^2} = 0 \quad (3.2c)$$

While this simplified set of equations can be solved analytically, it is still very tedious and computationally intensive. However, in formulating analytical vibrations problems, it is common to neglect the inertia in directions not corresponding to the primary direction of motion. For the case of a cylinder, the inertia in the axial and circumferential directions is often neglected, as motion is primarily in the radial direction. Assumptions such as this greatly simplify Eqs. 3.2. Consequently, the radial displacement component can be readily determined.

### 3.2 General Cylinder Vibrations

Before discussing the effect of these simplifications on the analytical solutions, the modal characteristics of cylindrical shells should be reviewed. The vibrations of cylindrical shells are typically defined as shown in Fig. 3.2 (from Ref. [3.1]). The mode shapes are generally identified by the number of waves ( $n$ ) around the circumference and the number of half-waves ( $m$ ) along the length. This notation is valid when both ends of the cylinder are prevented from moving radially. When one or both ends is radially free, the vibration pattern in the axial direction is usually identified using the number of nodal circles ( $m'$ ) along the length. It is also common to classify the mode shapes into three groups: axisymmetric modes ( $n=0$ ), in which the deformed shape is the same around the circumference; bending modes ( $n=1$ ), which are similar to transverse beam modes; and flexural ( $n>1$ ) modes.

The modal characteristics of shells are different from typical structures in that the simplest mode shapes (the ones with the fewest node lines) are not necessarily the lowest in frequency. This is illustrated by Fig. 3.3, which shows the frequency spectrum obtained by Forsberg [3.1] from the solution of Eqs. 3.1. For a given number of circumferential waves, the frequency increases with an increasing number of axial half waves (decreasing  $l/ma$ ). The lowest natural frequency will then always correspond to a mode with  $m=1$ . This behavior is typical of vibrating structures. However, the number of circumferential waves corresponding to the lowest frequency mode depends on geometrical features of the cylinder, such as the length to radius ratio, the radius to thickness ratio, and the end conditions. From Fig. 3.3, if  $l/a=10$ , the lowest mode will have  $m=1$  and  $n=4$ . However, if  $l/a=5$ , the lowest mode will have  $m=1$  and  $n=5$ . Of particular interest is the fact that the axisymmetric

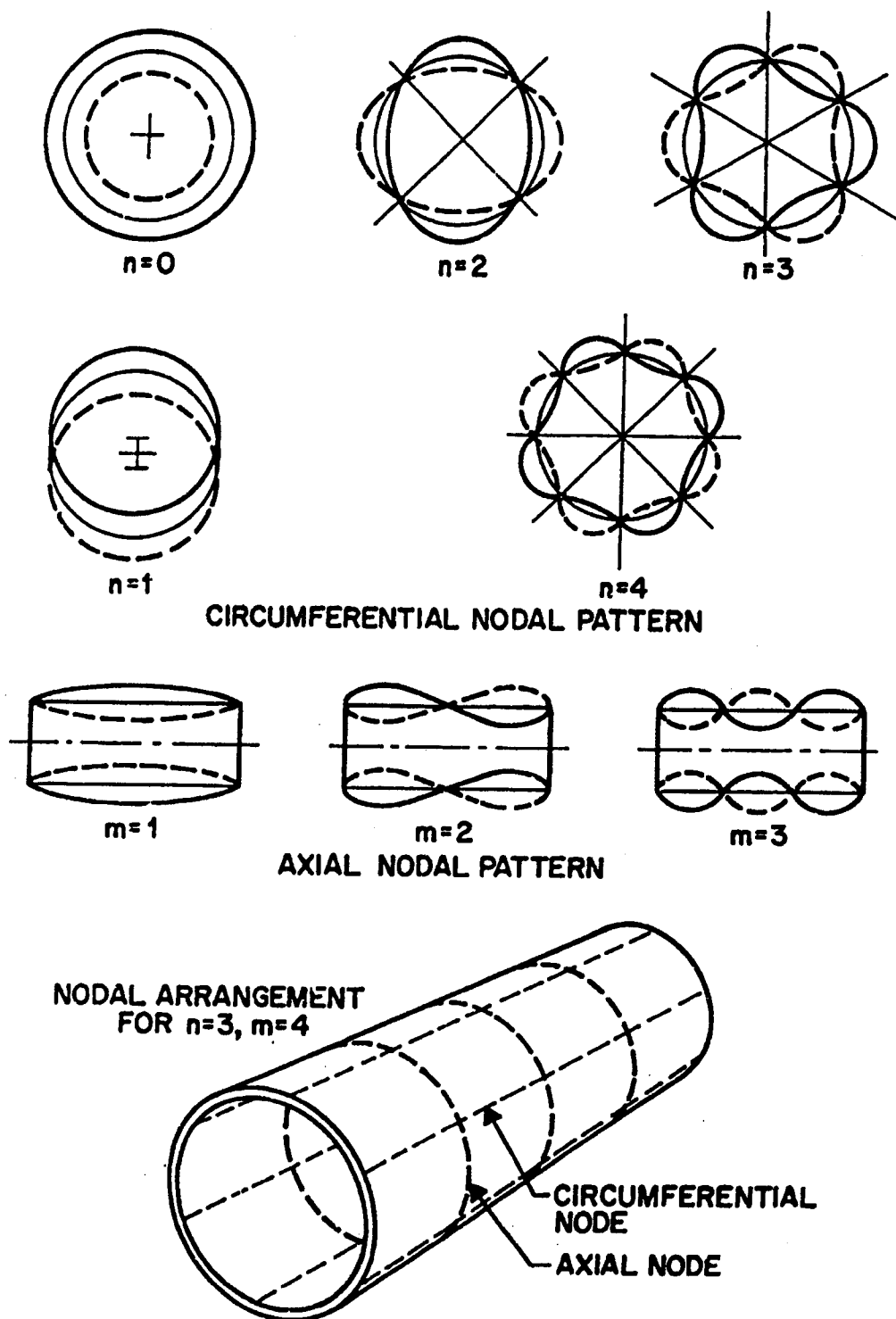


Fig. 3.2. Mode shapes of simply supported cylinders [3.1].

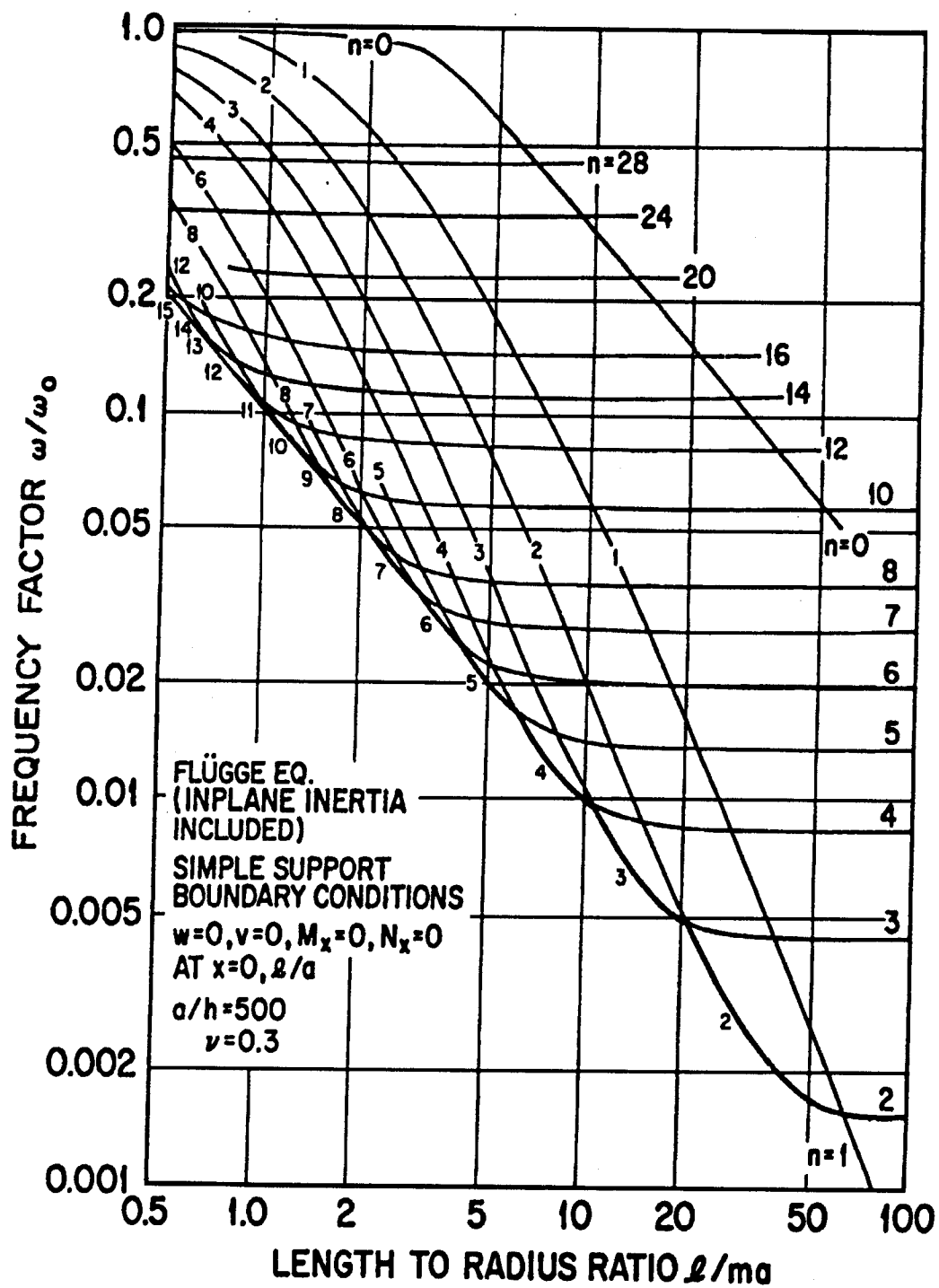


Fig. 3.3. Frequency spectrum for simply supported cylinders [3.1].

modes are relatively high in frequency. This is one reason that there has been little research on axisymmetric cylinder vibrations. High frequency modes require more energy to excite, so the  $n=0$  modes are not likely to respond unless the excitation is nearly axisymmetric.

It should be noted that the flexural ( $n>1$ ) modes are more dependent on  $a/h$  than the others; their modal frequencies tend to increase with increasing thickness. Thus for a shell with greater thickness, the curves for  $n>1$  in Fig. 3.3 would move upward relative to the curves for  $n=0$  and  $n=1$ . There would then be fewer flexural modes with frequencies below the lowest axisymmetric modes.

### 3.3 Axisymmetric Cylinder Vibrations

Since the problem that initiated this research was based on the axisymmetric blast loading of a cylinder, the initial literature search concentrated on this subject. Due to the relatively rare circumstances where this type of loading is encountered, literature on the subject is sparse. Two works on the subject by Powers [3.6] and Wang [3.7], though separated by 20 years, used the same basic procedure to solve this problem.

The general equations of motion (Eqs. 3.2) are initially simplified by removing all terms with a circumferential dependence. Since there can be no motion in this direction, the circumferential inertia term can also be neglected. With this, Eq. 3.2b drops out entirely and the remaining equations simplify to the following:

$$\frac{\partial^2 u}{\partial x^2} + v \frac{\partial w}{\partial x} - \gamma^2 \frac{\partial^2 u}{\partial t^2} = 0 \quad (3.3a)$$

$$k \frac{\partial^4 w}{\partial x^4} + v \frac{\partial u}{\partial x} + w + \gamma^2 \frac{\partial^2 w}{\partial t^2} = 0 \quad (3.3b)$$

Since the in-plane motion of shells is usually much smaller than the out-of-plane motion, it is often neglected to simplify the analysis. If the longitudinal inertia term of Eq. 3.2a is neglected, the resulting expression can be integrated once and the resulting expression for  $\partial u / \partial x$  substituted into Eq. 3.3b. The result is a fourth order differential equation given by

$$k \frac{\partial^4 w}{\partial x^4} + (1 - v^2)w + \gamma^2 \frac{\partial^2 w}{\partial t^2} = 0 \quad (3.4)$$

This equation is the same as that reported in Refs. [3.6] and [3.7] when differences in notation are corrected. If clamped boundary conditions (e.g.,  $u=w=\partial w/\partial x=0$ ) are applied to both ends, the following frequency equation results:

$$\cosh \lambda_i \cos \lambda_i - 1 = 0 \quad (3.5)$$

The frequency equation can be solved for the eigenvalues ( $\lambda_i$ ), and the natural frequencies are then given by

$$\omega_i^2 = \frac{E}{\rho} \left( \frac{h^2}{12l(1-v^2)} \lambda_i^4 + \frac{1}{a^2} \right) \quad (3.6)$$

The lowest extensional frequency of a ring can be used to non-dimensionalize the frequency parameter. This removes the effect of material properties from the presentation of frequency results. This frequency parameter is defined as

$$\omega_o = \frac{1}{a} \left[ \frac{E}{\rho(1-v^2)} \right]^{1/2} \quad (3.7)$$

The resulting frequency curves are shown in Fig. 3.4 for different values of  $a/h$ . The curves converge as they approach  $\omega/\omega_0=1$ . This behavior is expected, as the extensional ring frequency ( $\omega_0$ ) is independent of the thickness. For higher  $l/ma$  ratios the curve is nearly horizontal, which indicates that for long shells the modes with the lowest number of axial waves can be very close in frequency. However, when finite elements were used to verify these results, discrepancies were found. In order to determine the cause, a more thorough investigation into the axisymmetric equations of motion was undertaken.

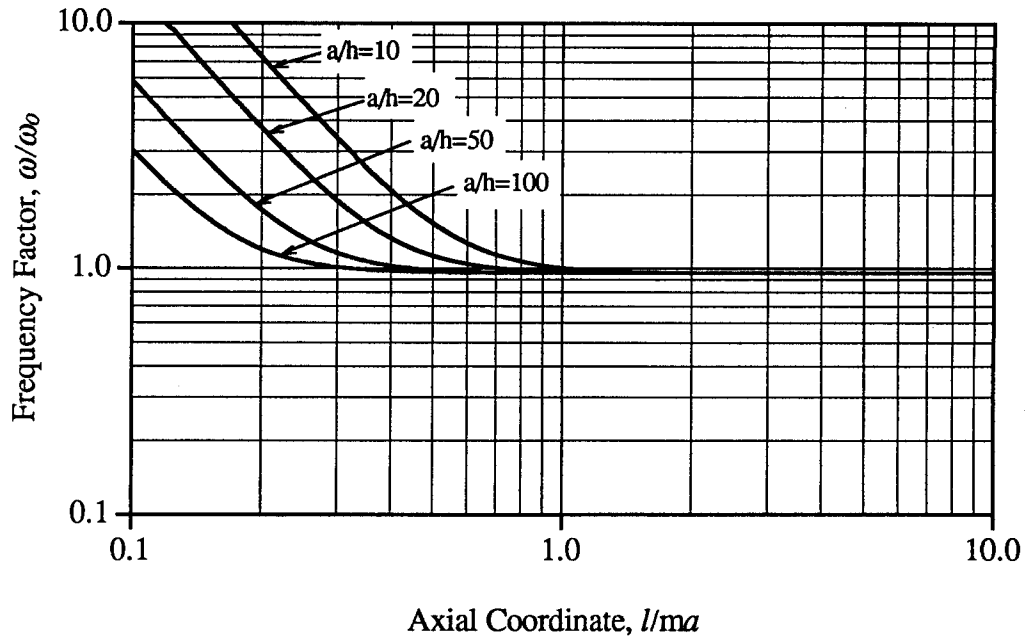


Fig. 3.4. Frequency spectrum for  $n=0$  with longitudinal inertia neglected.

### 3.4 Effect of Neglecting Longitudinal Inertia

The most significant research in this area was that of Forsberg [3.1, 3.5]. He solved the general equations of motion (Eqs. 3.1) for the axisymmetric case and investigated the effects of various assumptions [3.1]. He showed that for the

axisymmetric case, the general equations of motion break down into two sets. One is a second-order system describing torsional motion. This case will not be discussed here. The second is a sixth-order system involving radial and longitudinal motion (coupled). He solved this system and showed that the resulting frequency spectrum (see Fig. 3.5) is quite interesting. The two frequency curves are asymptotic to two lines, one horizontal and one diagonal. As previously mentioned, the horizontal line at  $\omega/\omega_0=1$  corresponds to the extensional ( $n=0$ ) frequency of a ring. As the frequency curves approach this line the mode shapes consist of primarily radial motion. The diagonal line corresponds to longitudinal bar vibrations; as the curves approach this line the mode shapes are dominated by longitudinal motion. In between these two extremes, the mode shapes contain significant amounts of both longitudinal and radial motion. In this region the displacement components are coupled, so a radial excitation can induce significant longitudinal motion and vice versa. For this reason errors will result if the longitudinal inertia is neglected.

However, the resulting errors may not be too severe depending on the accuracy required. It was mentioned that for non-axisymmetric cylinder vibrations, the solution of the frequency equation results in three distinct frequencies for each nodal pattern, where each frequency corresponds to a mode with different relative magnitudes of the three displacement components. In the axisymmetric case, the two frequency curves represent the two distinct frequencies for each mode shape, where the two frequencies correspond to modes with the same number of axial half-waves but different relative magnitudes of radial and longitudinal displacements. If the axial inertia is neglected, only one frequency for each mode will be present, and the mode shapes will not have significant axial motion. Depending on the  $l/a$  ratio, the modes that are missed may not contain significant radial motion, and would



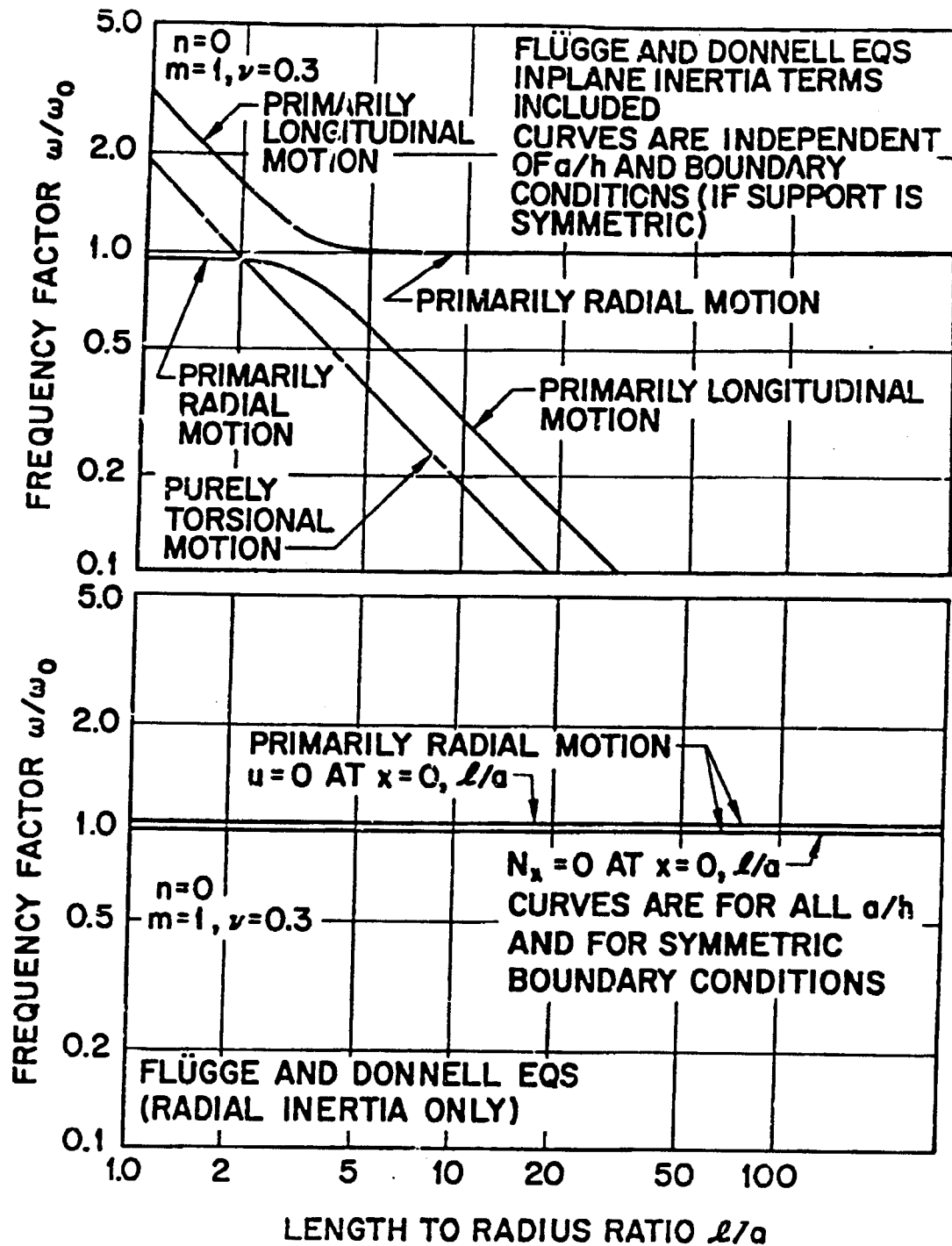


Fig. 3.5. Frequency spectrum for  $n=0$ , with and without longitudinal inertia [3.1].

contribute little to the radial response of the cylinder. This is illustrated by close comparison of Figs. 3.4 and 3.5.

### 3.5 Effect of End Conditions

Forsberg also investigated the effect of various end conditions on the axisymmetric vibrations of cylinders [3.5]. He showed that only the axial restraint has a significant effect on the frequency, as shown in Fig. 3.6. For regions where there is significant axial motion, an axial restraint at one end will cause the minimum frequency to be approximately one half of that with no axial restraint. In addition, if there is axial restraint at both ends, the frequencies will be the same as if there were no axial restraints. Contrary to what would be expected, the radial restraint has very little effect ( $<0.5\%$ ) on the frequency.

While the end conditions may have little effect on the frequency (if they are the same at both ends), they may have a significant effect on the appearance of the mode shapes. Figure 3.7 shows the lowest axisymmetric mode as obtained by Forsberg [3.5] for the case where  $a/h=20$  and  $l/a=5$ . For the first set of boundary conditions (plotted with the solid line) only radial restraint is applied, while for the second set (plotted with the dashed line) radial and axial restraints are applied. In both cases the restraints are symmetric (same at both ends). Note that when axial restraint is applied, the longitudinal displacements undergo a  $90^\circ$  phase shift in order to fulfill the requirement that  $u=0$  at the ends. The radial displacements also shift by  $90^\circ$ , and the requirement that  $w=0$  is met by localized distortions at the ends. These distortions propagate far along the length due to the relative thickness ( $a/h=20$ ) of the shell. This effect may cause great confusion in attempting to identify the modes.

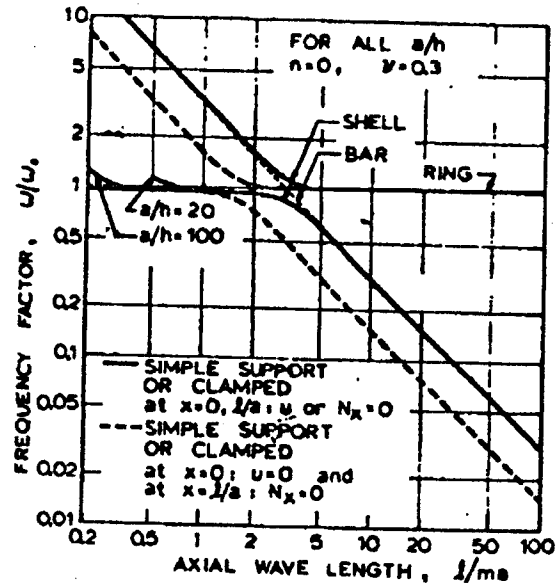


Fig. 3.6. Effect of end conditions on the frequency spectrum for  $n=0$  [3.5].

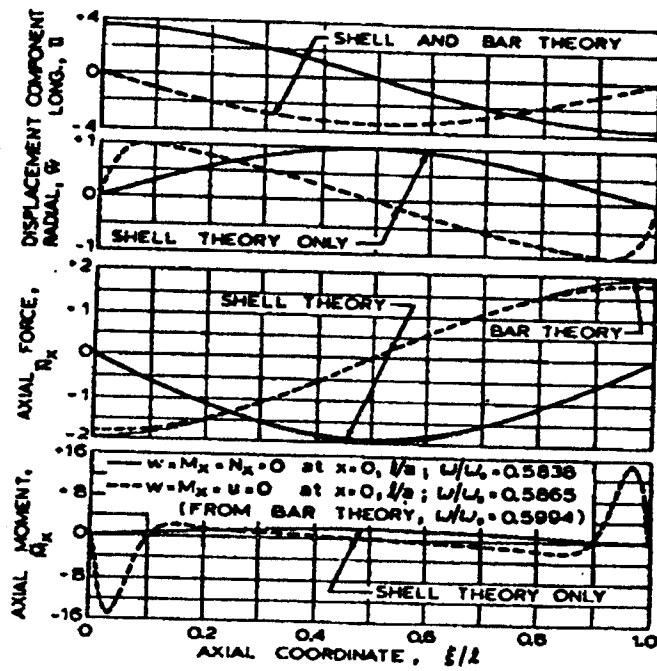


Fig. 3.7. Mode shape and force distributions for lowest axisymmetric mode [3.5].

While mathematically the number of axial half-waves is only one, the mode shape definitely appears to have two axial half-waves. As noted by Goldman [3.8], this mode is not symmetric about the mid-span, and therefore would not respond to a uniform radial blast load. He argues that the mode should be labeled  $m=2$ . However, this conflicts with the use of  $l/ma$  in presenting frequency results.

The localized distortion also causes a large increase in the bending moment near the ends of the shell (Fig. 3.7). Forsberg noted that the maximum bending moment was still only about 20% of the maximum hoop stress. However, this amount of stress may still be of concern, so it is important that the mode shapes be accurately represented.

### 3.6 References

- [3.1] Forsberg, K., "A Review of Analytical Methods Used to Determine the Modal Characteristics of Cylindrical Shells," NASA CR-613, 1965.
- [3.2] Leissa, A. W., *Vibration of Shells*, NASA SP-288, 1973.
- [3.3] Flügge, W., *Stresses in Shells*, Springer-Verlag, Berlin, 1960, Chap. 5, pp. 219-233.
- [3.4] Donnell, L. H., "Stability of Thin-Walled Tubes Under Torsion," *Twentieth Annual Report of the National Advisory Committee for Aeronautics*, Report No. 479, United States Government Printing Office, Washington, D.C., 1935, pp. 95-116.
- [3.5] Forsberg, K., "Axisymmetric and Beam-Type Vibrations of Thin Cylindrical Shells," *American Institute of Aeronautics and Astronautics Journal*, Vol. 7, No. 2, Feb. 1969, pp. 221-227.
- [3.6] Powers, J. P., "Structural and Fatigue Analysis of the Sandia Laboratory Microfusion Reaction Chamber," M.S. thesis, 1991, University of Wisconsin-Madison, Madison, WI.
- [3.7] Wang, J. T., Stadler, W., and Lin, C., "The Axisymmetric Response of Cylindrical and Hemispherical Shells to Time-Dependent Loading," NASA CR-572, 1966.

- [3.8] Goldman, R. L., "Mode Shapes and Frequencies of Clamped-Clamped Cylindrical Shells," *American Institute of Aeronautics and Astronautics Journal*, Vol. 12, No. 12, Dec. 1974, pp. 1755-1756.

## Chapter 4

### Finite Element Modal Analysis

Due to the complexity of the analytical solution, it is very difficult to obtain the vibration characteristics of cylinders even for the simplest cases with ideal boundary conditions. Handling complications such as end rings, perforations, and such would be virtually unthinkable using analytical methods. Experimental techniques are feasible, but can be very expensive and time consuming. This is especially true when many design iterations are necessary. The emergence of finite element methods in the past few decades has revolutionized the analysis of structures. It is now much easier to accurately predict the behavior of complex systems.

The ultimate goal of this research was to develop accurate finite element modeling techniques to be used in designing ICF target chambers. However, the unexpected results obtained while verifying basic cylinder models led to an in-depth investigation of the axisymmetric modal characteristics of cylinders.

#### 4.1 Modeling

The commercial finite element code ANSYS® [4.1] was used throughout this investigation. In order to verify results within ANSYS, several different methods were used to model the cylinder. Two basic types of models were implemented, axisymmetric and non-axisymmetric. The non-axisymmetric models will be referred to as "slice" models, as they were used to model varying circumferential amounts of the cylinder, i.e., 30°, 90°, 360°, etc. A very small slice (1-2°) is similar to an axisymmetric model. The following types of elements all gave results that

converged within a few percent: two-node axisymmetric shell, four-node axisymmetric solid, four-node plate/shell, and eight-node isoparametric solid.

Two methods were used to solve for the mode shapes and natural frequencies. The full subspace method uses the full stiffness and mass matrices, thus including every nodal degree of freedom as unknowns. This produces the most accurate results, but can be very time consuming. For dynamic analyses, very accurate results can usually be obtained much faster through the use of a reduced subspace method. This procedure reduces the size of the stiffness and mass matrices by in effect lumping the mass at master degrees of freedom (mdofs). However, care must be taken when selecting the mdofs. As noted in the previous chapter, the cylinders in this study have significant motion in the axial direction, as well as the expected radial motion. Thus, axial mdofs must be selected as well as radial mdofs in order to obtain correct results. It was found that serious errors can result from a failure to do this.

## 4.2 General Cylinder Vibrations

A half-circumference symmetry ( $180^\circ$  slice), four-node shell element model of a cylinder was used to verify the finite element modeling techniques. The following dimensions and material properties were chosen to match the example given by Vronay and Smith [4.2]:  $l = 12.0$  in.,  $a = 3.0$  in.,  $h = 0.01$  in.,  $E = 29.6 \times 10^6$  psi,  $\nu = 0.29$ ,  $\rho = 0.733 \times 10^{-3}$  lb-sec<sup>2</sup>/in<sup>4</sup>. The model is shown in Fig. 4.1. The end conditions for this example are completely clamped, which means there is no translation or rotation at the ends ( $u=v=w=\partial w/\partial x=0$ ). The use of symmetry results in some modes not being found, as the mode shape must be compatible with the

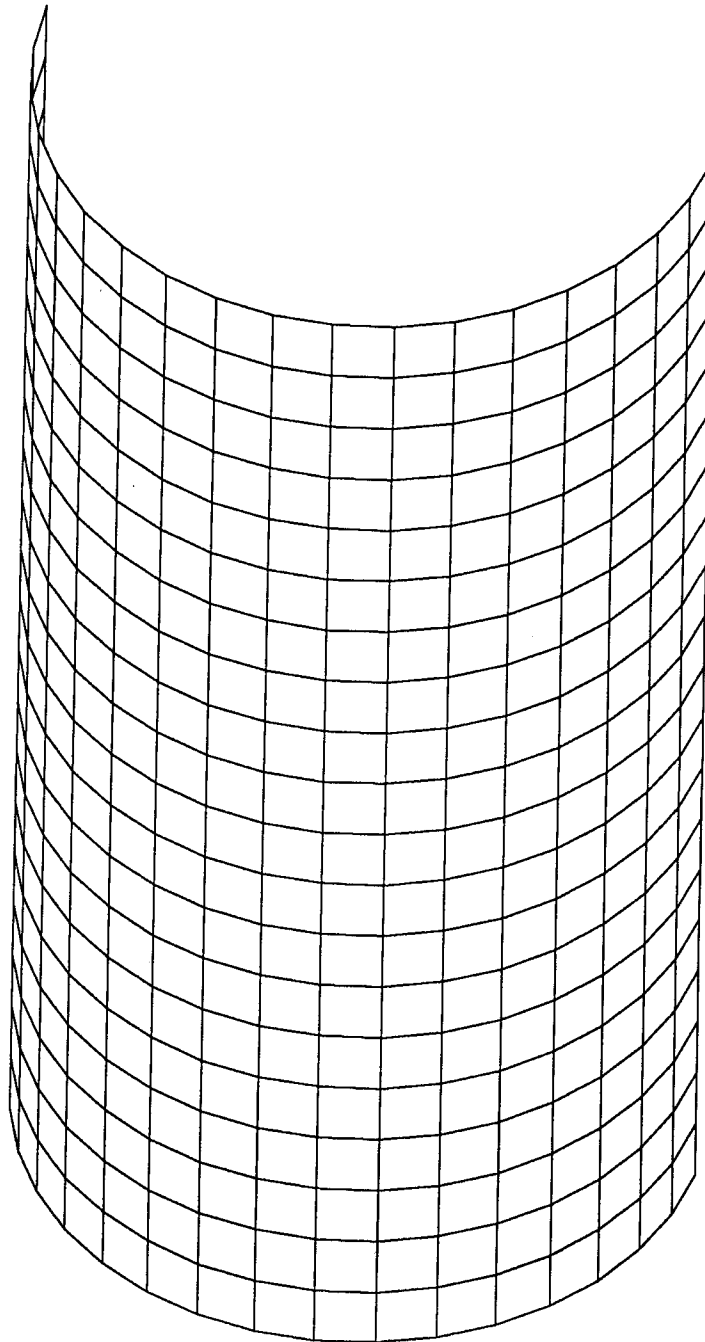


Fig. 4.1. Half cylinder finite element model.



boundary conditions used to enforce symmetry. The symmetry boundary conditions are: no circumferential translation and no rotation about the edge of symmetry. For a half model of a cylinder, the only modes that will not be found are those which are primarily torsional.

A deformed mesh plot of the lowest mode is shown in Fig. 4.2. Determining the mode shape from plots such as this can be difficult, particularly with higher modes. A contour plot of the radial displacements provides an easier way to identify the modes. If the half model of the cylinder is "unrolled" and laid flat, the contour plot of Fig. 4.3 results. Note that the contour levels represent the relative radial displacements of the cylinder wall. One half wave is visible in the axial direction, and three waves in the circumferential direction. This corresponds to a mode shape with  $m=1$  and  $n=6$ . Table 4.1 compares the frequencies for several modes with the results given in Ref. [4.2]. The results compare very well, verifying the meshing density and the type of finite element used in the model.

Table 4.1. Comparison of finite element and analytical [4.2] modal frequencies.

m	Source	n				
		3	4	5	6	7
1	Analytical	1154	765	581	539	599
	Finite Element	1159	767	580	533	589
2	Analytical		1752	1287	1022	908
	Finite Element		1767	1302	1034	913
3	Analytical				1719	1431
	Finite Element				1751	1461

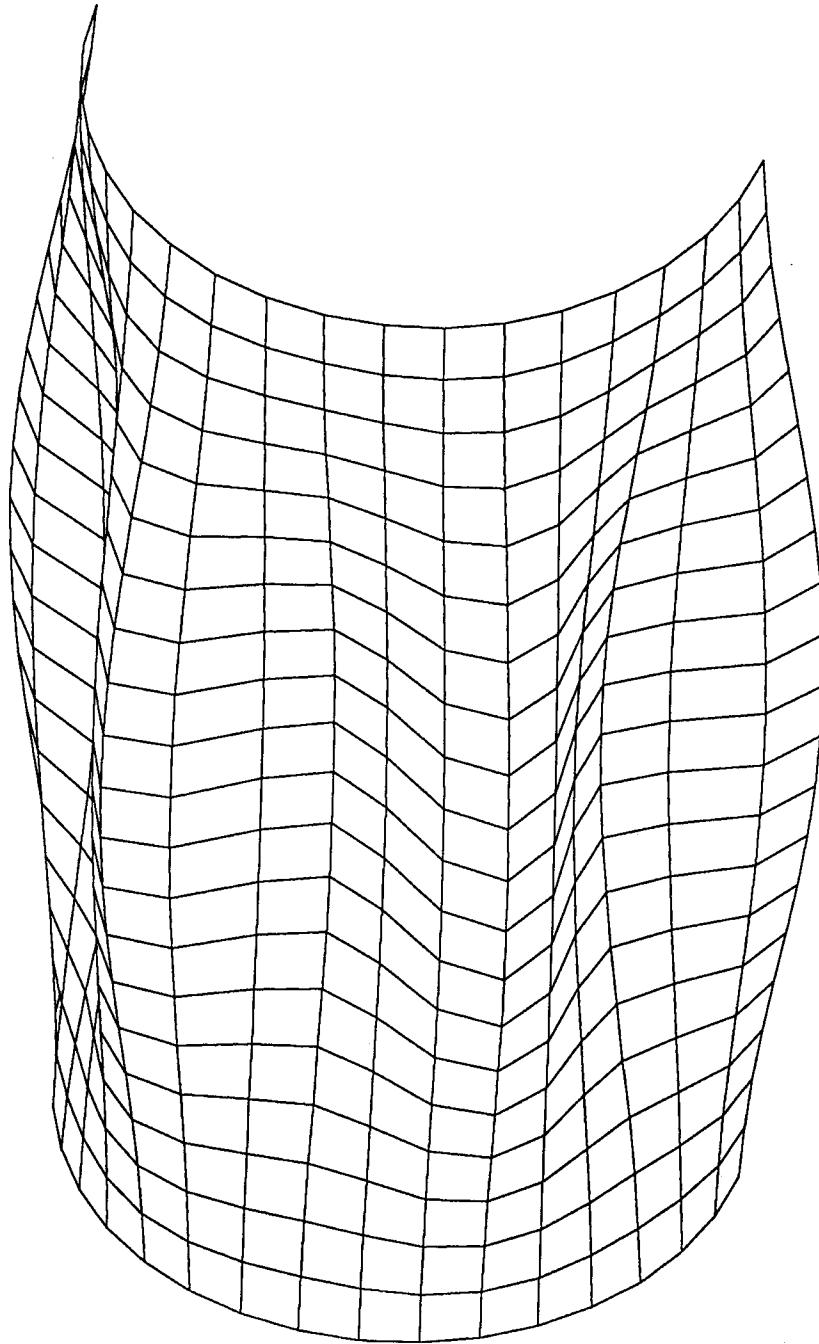


Fig. 4.2. Deformed mesh plot showing the mode shape  $m=1$  and  $n=6$ .

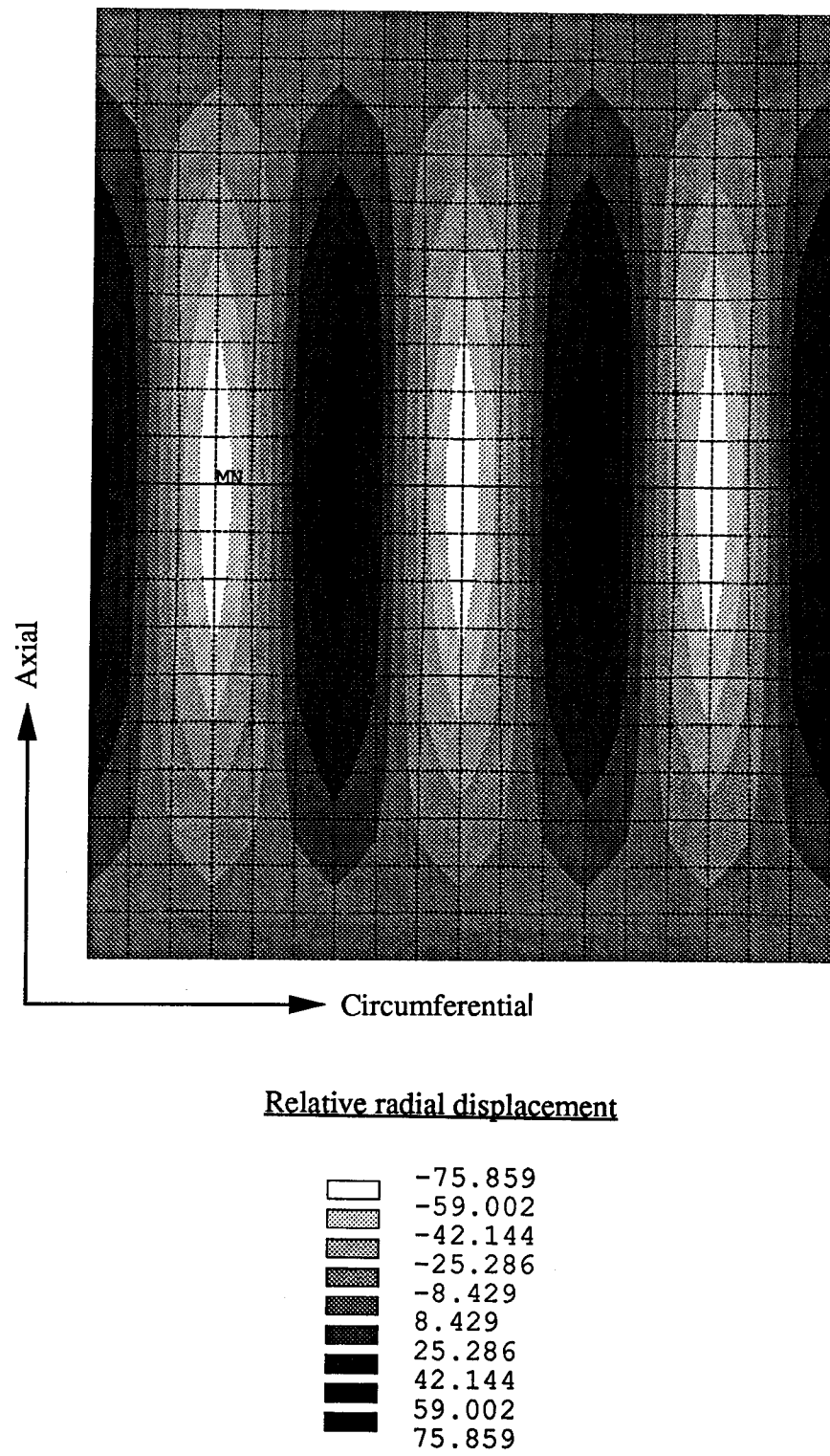


Fig. 4.3. Contour plot of radial displacements for the  $m=1$  and  $n=6$  mode shape.

### 4.3 Axisymmetric Cylinder Vibrations

As mentioned in Chapter 3, the axisymmetric ( $n=0$ ) modes are generally very high in the frequency spectrum. For the cylinder used in the example above, the first axisymmetric mode occurs at 7981 Hz, and the mode shape is shown in Fig. 4.4. Because the modal displacements are the same all the way around the circumference, this symmetry can be exploited to lead to much simpler finite element models. One method is to model a very small ( $1-5^\circ$ ) slice of the cylinder, using the same symmetry conditions as in the  $180^\circ$  model. An even greater simplification results by using axisymmetric elements formulated especially for this purpose. These elements reduce the problem from three dimensions to two dimensions, which greatly reduces the size and complexity of the solution.

Figure 4.5a shows the first mode from a two-node axisymmetric shell element model using the same dimensions, material properties, and end conditions as the previous example. The axisymmetric mode shape is like a cross-sectional view of the deformed cylinder shown in Fig. 4.4, with the straight line representing the undeformed cylinder wall (note that the cylinder axis is horizontal, whereas in Fig. 4.4 it was vertical). The frequency of 7993 Hz from the axisymmetric model is within 0.15 percent of the 7981 Hz result from the  $180^\circ$  model, indicating excellent agreement between modeling methods. Goldman [4.3] also solved this example analytically and obtained a frequency of 8017 Hz for this mode, which agrees with the finite element results within less than half a percent. The mode shape also compares well; his results are shown in Fig. 4.5b (see curve labeled  $n=0$ ).

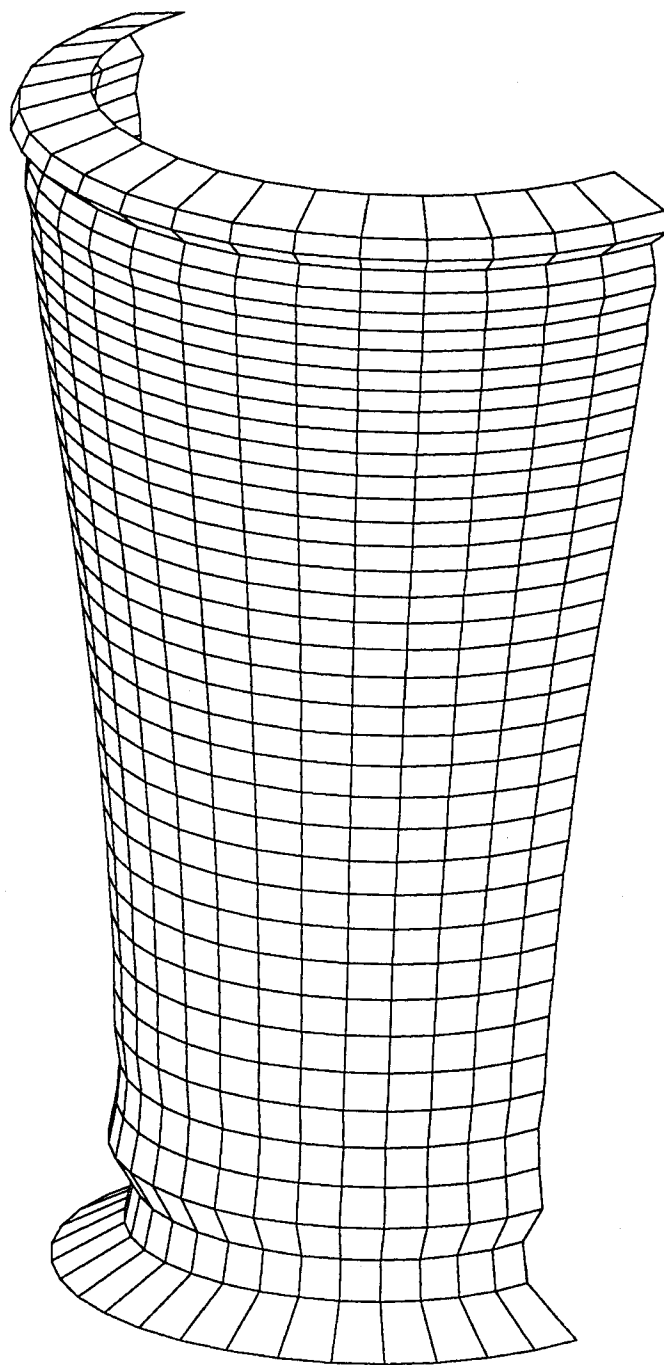
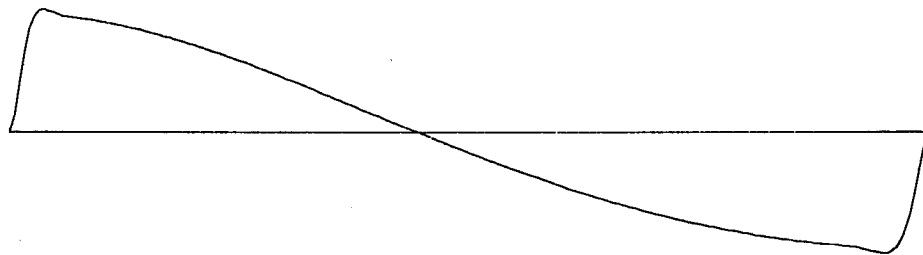
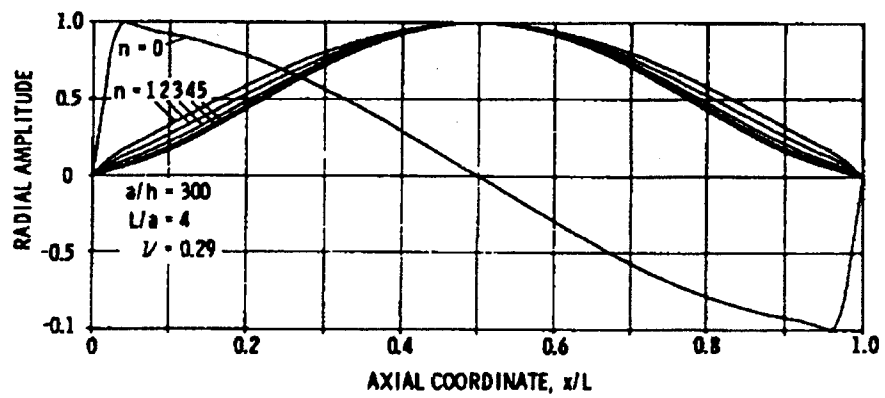


Fig. 4.4. Deformed mesh plot of lowest axisymmetric mode from half cylinder model ( $m=1$ ,  $n=0$ ).



(a) Finite element results ( $m=1, n=0$ ).



(b) Analytical results [4.3] ( $m=1$ ).

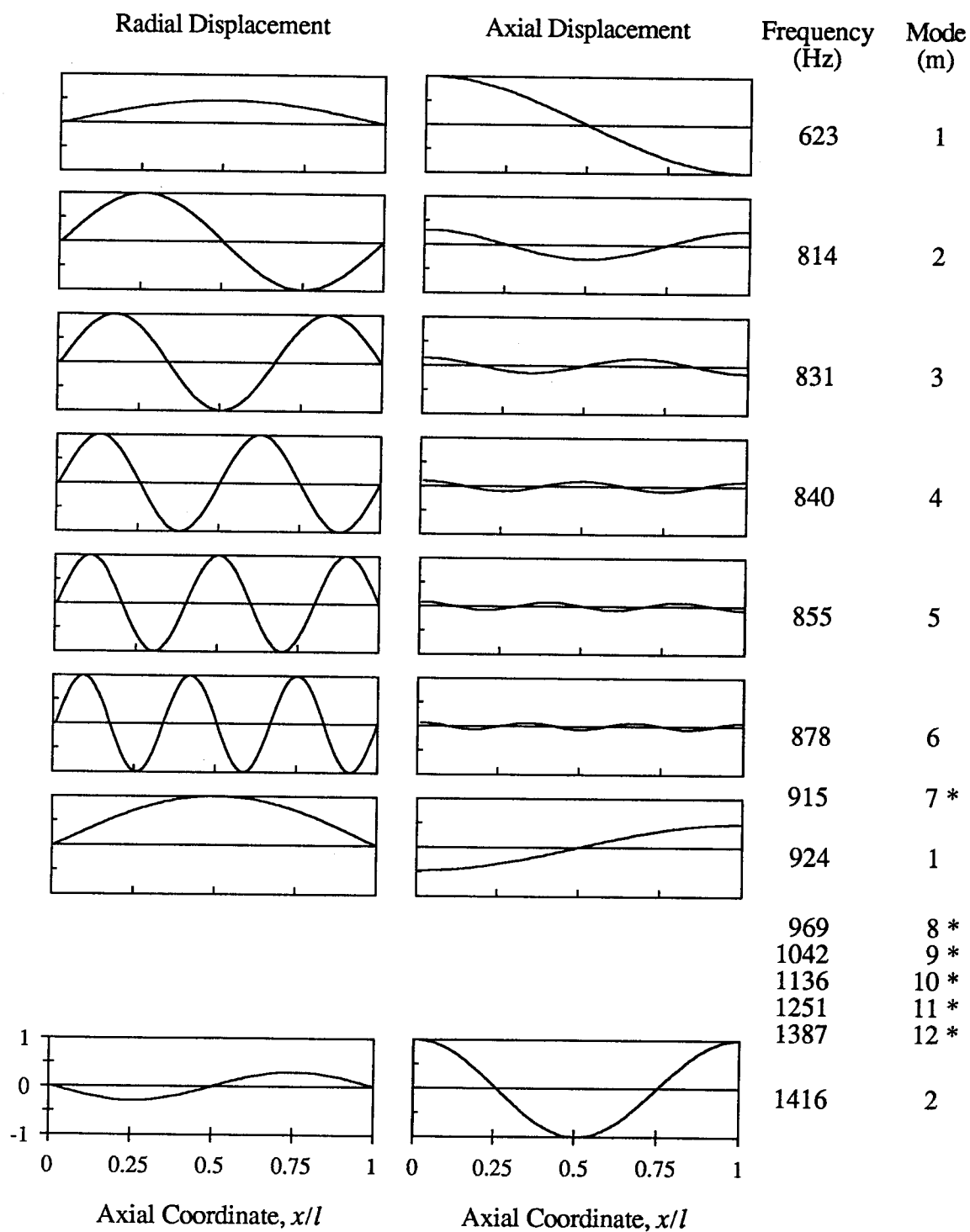
Fig. 4.5. Comparison of finite element and analytical [4.3] results for lowest axisymmetric mode.

Due to their simplicity, the two-node axisymmetric elements were used to investigate the effects of shell dimensions and end conditions on the mode shapes and frequencies. The two node elements are intended primarily for thin shells, but they performed quite well even for relatively thick shells. To ensure accurate results, four-node axisymmetric elements were used to verify the two-node models when the shells under investigation were relatively thick.

#### 4.4 Effect of Cylinder Dimensions

The effect of the cylinder dimensions on the modal characteristics was studied using simply supported end conditions (i.e.,  $w=0$ ). Analytical results for this were presented in Chapter 3, but it serves as a verification and a useful illustration of the results. The material properties used were:  $E = 216 \text{ GPa}$ ,  $\nu = 0.3$ ,  $\rho = 7800 \text{ kg/m}^3$ . The radius was fixed at 1 m, and the length and thickness were varied to obtain the desired  $l/a$  and  $a/h$  ratios. This yields a value for the frequency parameter,  $\omega_o=876 \text{ Hz}$ . The mode shapes and frequencies for  $l/a=4$ ,  $a/h=20$  are shown in Fig. 4.6. Note that the radial and axial displacement components have been plotted separately, side by side. The mode shapes are scaled so that the larger of the two displacement components is normalized to unity. The modes are shown in order of increasing frequency, but not all modes have been plotted. The omitted modes followed the existing trend in displacement shape and varied only in the number of waves.

The general trend in mode shapes is the same as that outlined previously in Section 3.4 and shown in Fig. 3.5. For the first mode shape (frequency=622 Hz) the radial and axial displacements both have one half wave along the length of the



\* Mode shape not illustrated

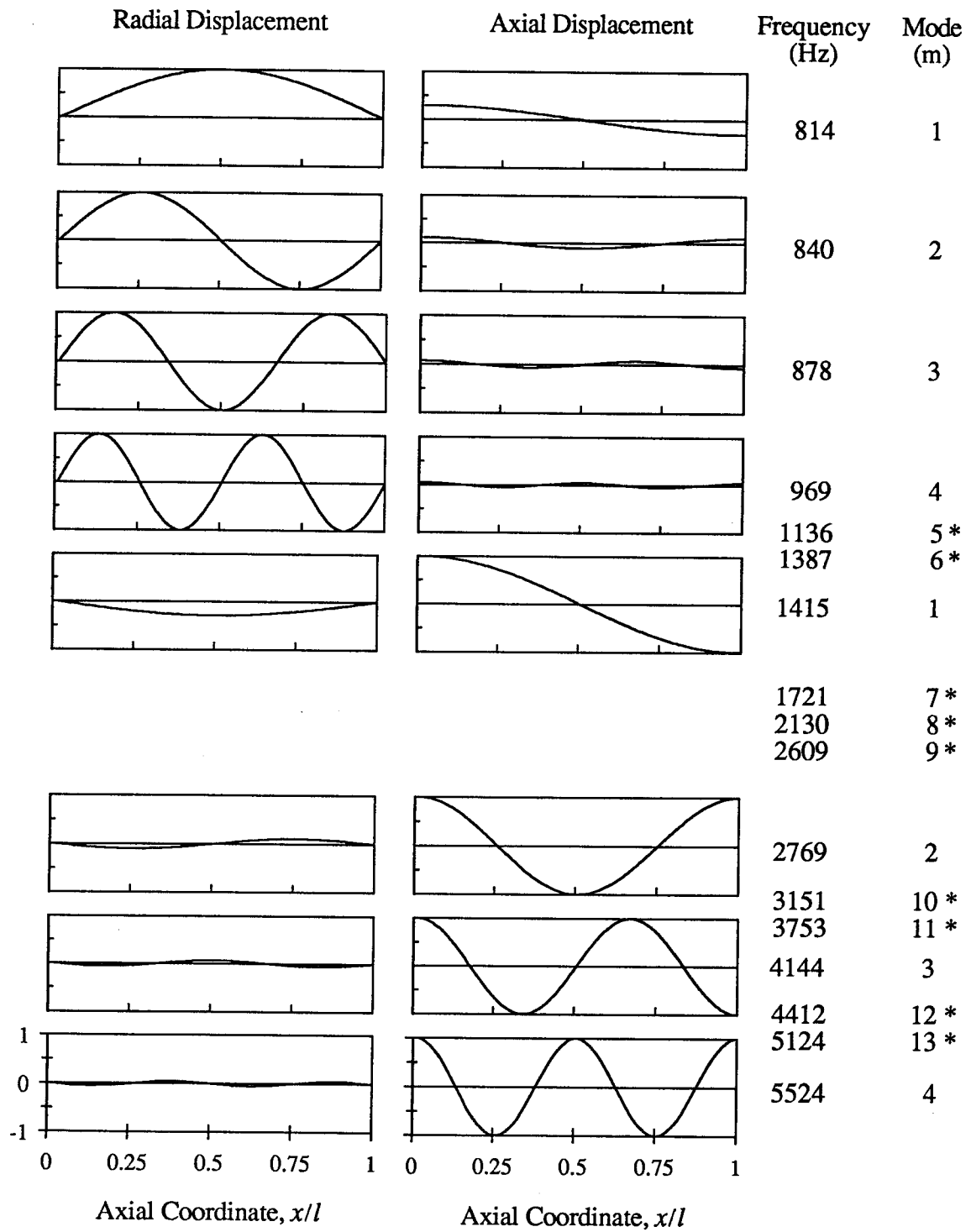
Fig. 4.6. Mode shapes with  $l/a=4$ ,  $a/h=20$  (simply supported end conditions).



cylinder, but the axial component is shifted  $90^\circ$  in phase. The axial displacement is larger than the radial, which is expected for a mode on the lower frequency curve (Fig. 3.5) with  $l/ma=4$ . The next mode has two axial half waves, which corresponds to  $l/ma=2$ . As shown in Fig. 3.5, when the low frequency curve is followed in the direction of decreasing  $l/ma$  (increasing  $m$ ), the mode shape will have proportionately more radial motion. This is reflected in the relative magnitudes of the radial and axial components in the second mode of Fig. 4.6. The next several modes follow the trend of increasing radial motion, and the frequencies become more closely spaced as  $\omega/\omega_0$  approaches unity. The mode at 924 Hz is the second  $m=1$  mode, which corresponds to  $l/ma=4$  on the upper frequency curve in Fig. 3.5. Several more modes from the lower frequency curve are picked up before the next mode (1416 Hz,  $m=2$ ) on the high frequency curve. The plots of the two modes on the high frequency curve illustrate the relative increase in the axial displacement component as  $l/ma$  is decreased.

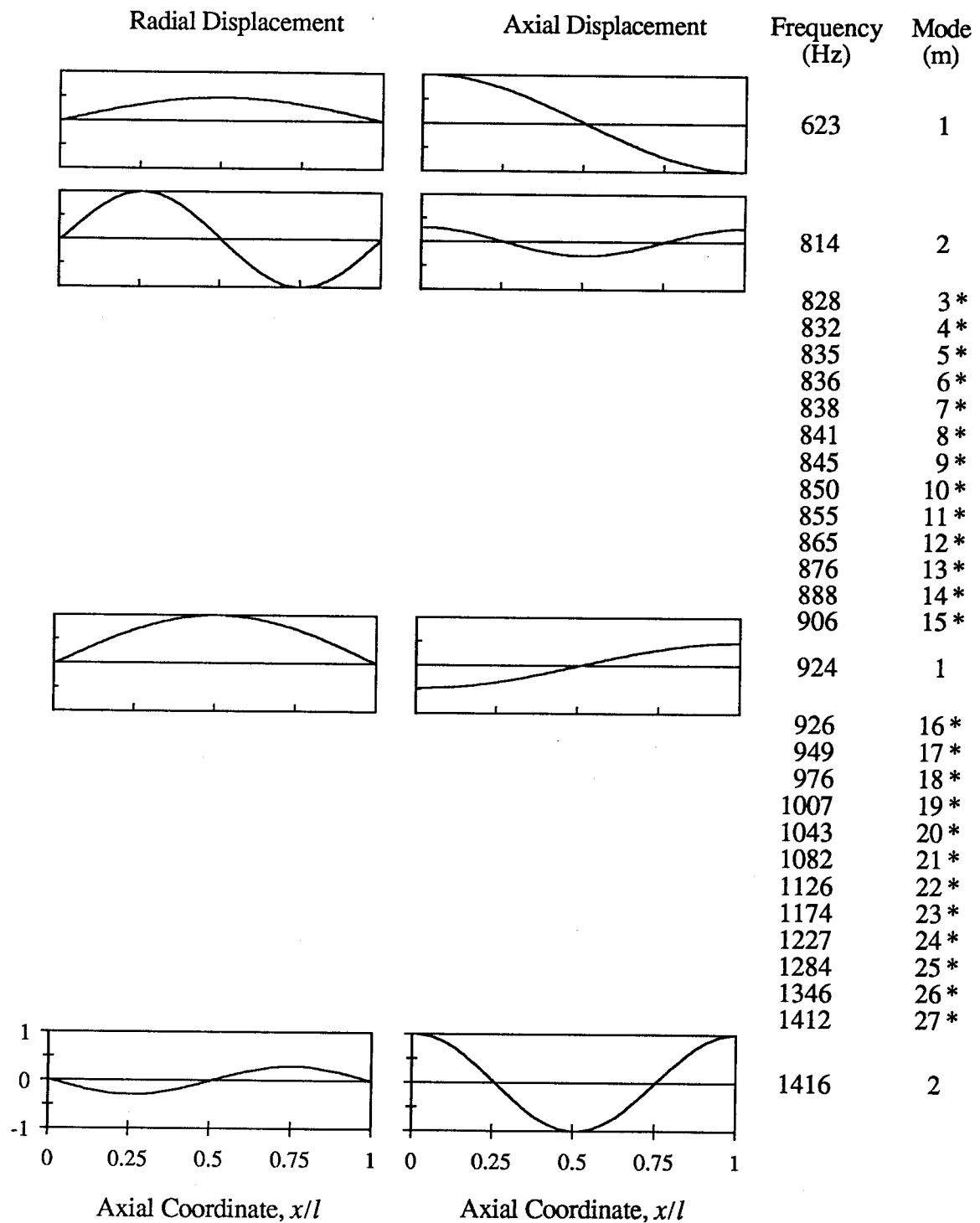
The mode shapes and frequencies for  $l/a=2$ ,  $a/h=20$  are shown in Fig. 4.7. The modal characteristics are very similar to those just discussed. The validity of nondimensionalizing using the axial wave length ( $l/ma$ ) is demonstrated by comparing the first mode here to the second mode from  $l/a=4$  (Fig. 4.6). Because one axial half wave is the same length for these modes, the frequency is the same. Also illustrated is the fact that the radial to axial displacement ratio is a function of  $l/ma$ , as the ratio is the same for these two modes.

The mode shapes and frequencies for  $l/a=2$ ,  $a/h=100$  are shown in Fig. 4.8. They can be compared to those in Fig. 4.6 to see the effect of wall thickness. As found by previous investigators, the wall thickness only affects the lower curve of the



\* Mode shape not illustrated

Fig. 4.7. Mode shapes with  $l/a=2$ ,  $a/h=20$  (simply supported end conditions).



\* Mode shape not illustrated

Fig. 4.8. Mode shapes with  $l/a=4$ ,  $a/h=100$  (simply supported end conditions).

frequency spectrum below  $l/ma = 1$ . This is illustrated by the fact that the lowest modes in Figs. 4.6 and 4.8 have nearly identical frequencies, but as  $m$  increases the frequencies start to diverge.

The results of these three sets of parameters, along with many others, were used to produce Fig. 4.9. This is a plot of the frequency spectrum for  $n=0$ , with the same format as Figs. 3.5 and 3.6. The results agree very closely with those plots.

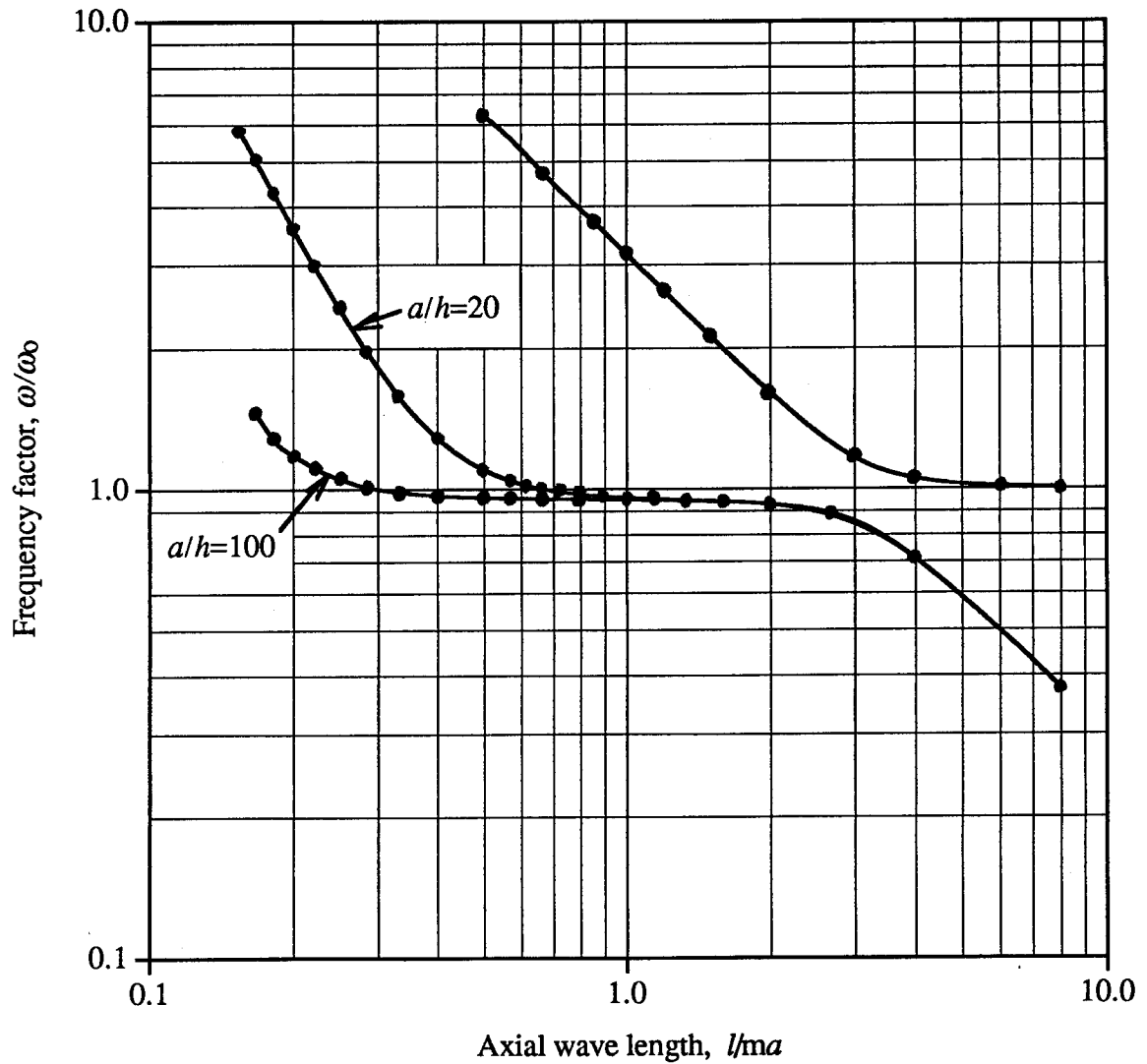
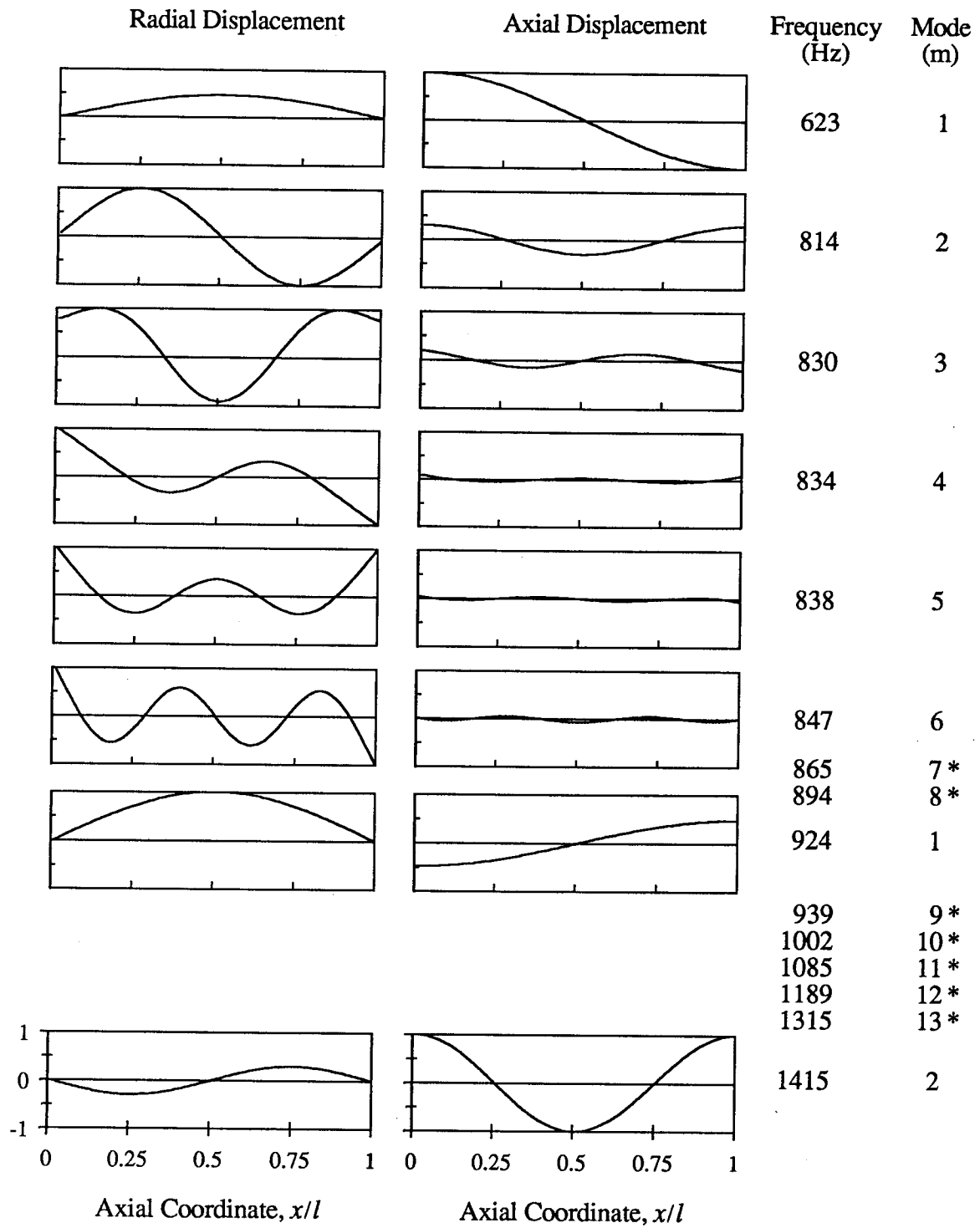


Fig. 4.9. Frequency spectrum for  $n=0$  from finite element models (simply supported end conditions).

## 4.5 Effect of End Conditions

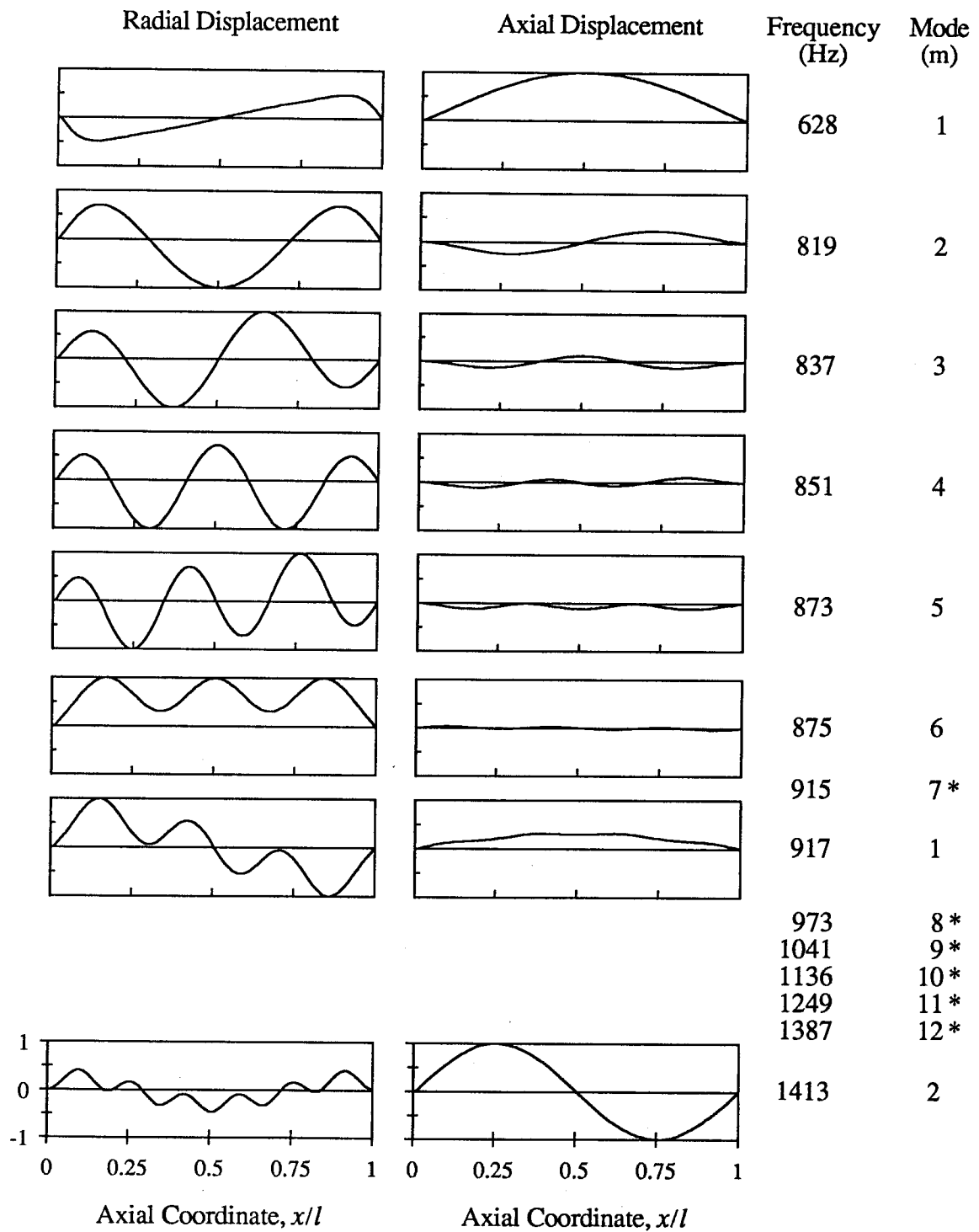
To determine their effects on the modal characteristics, the end conditions were first varied with all other parameters held constant. The results from the case of  $l/a=4$ ,  $a/h=20$ ,  $w=0$  (Fig. 4.6) are used as the baseline, and will be referred to as the radially restrained case. When the radial restraints are removed, the result is free end conditions. The resulting mode shapes are shown in Fig. 4.10. Forsberg [4.4] stated that "a shell which is force-free at the boundary has essentially the same modal characteristics as one which is radially restrained but force-free". While this is true for the two lowest modes, as seen by comparing Figs. 4.6 and 4.10, this is not true for the higher modes. While the radial displacement at the ends is nearly zero for the first two modes, the free end conditions result in very different mode shapes for the remaining modes. If the regions between the ends of the cylinder and the first radial displacement zero crossings are taken as axial half waves, the number of half waves corresponds to those for the radially restrained case. As  $m$  is increased, the frequencies for the radially restrained case increase slightly faster than those for the free case, with a difference of 6% at  $m=7$ .

When both the axial and radial restraints were added, the modes in Fig. 4.11 were obtained. The results for the first mode are similar to those given in Fig. 3.7; the radial and axial displacements both shift  $90^\circ$  along the length from the radially restrained case (Fig. 4.6), and the axial displacement is distorted at the ends so that  $w=0$ . As mentioned previously, confusion can arise over whether this should be called the  $m=1$  or  $m=2$  mode. It is the opinion of the author that the  $m=1$  notation is correct. This interpretation allows the use of the dimensionless axial half wave



\* Mode shape not illustrated

Fig. 4.10. Mode shapes with  $l/a=4$ ,  $a/h=20$  (free end conditions).



\* Mode shape not illustrated

Fig. 4.11. Mode shapes with  $l/a=4$ ,  $a/h=20$  (end conditions  $u=w=0$ ).

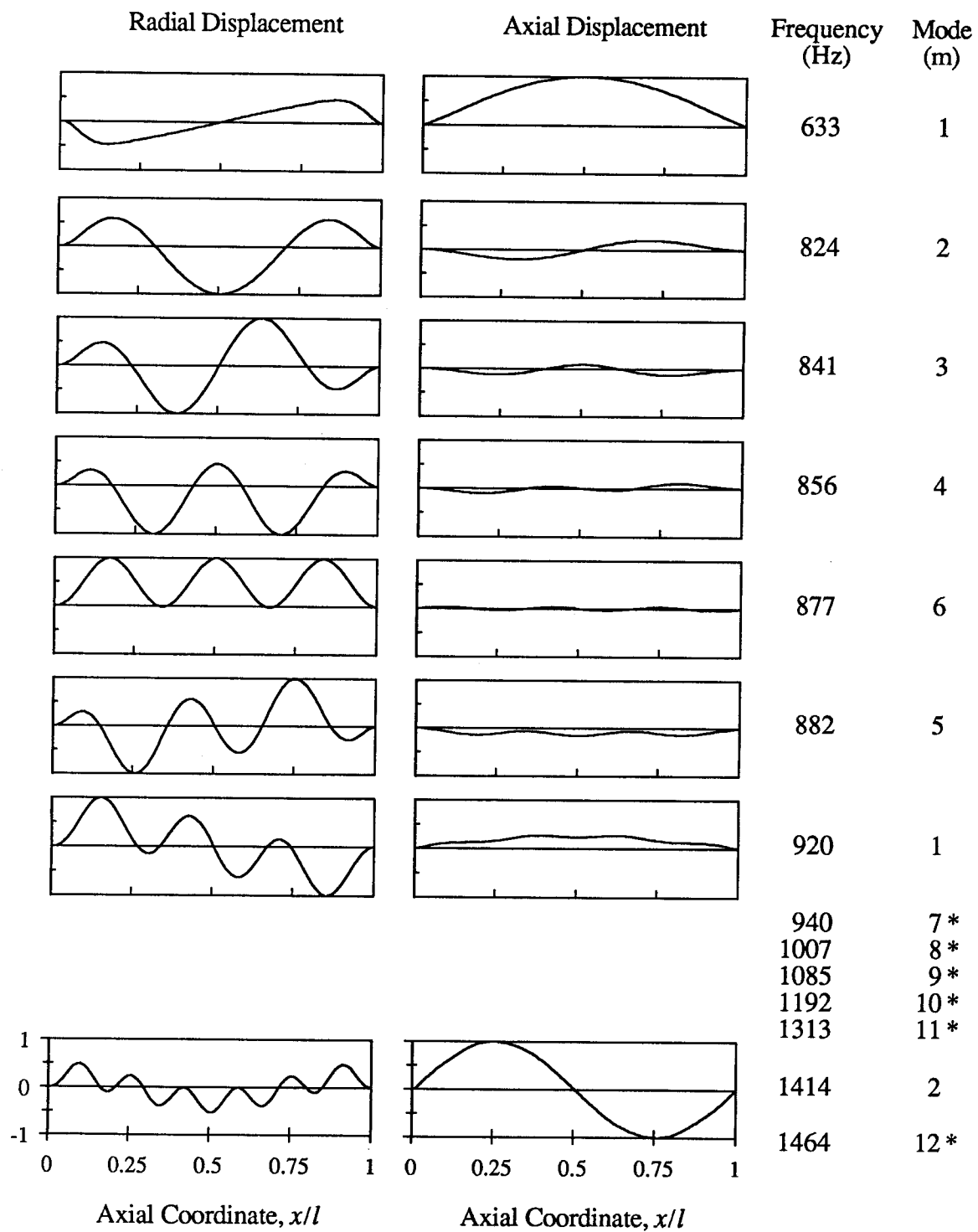
length  $l/ma$  in plotting results, and also causes the axial and radial displacements to more consistently have the same number of half waves ( $m$ ). This allows one to make sense of the otherwise extremely confusing appearance of the higher modes. The first anomaly is noticed in the fifth mode at 873 Hz. The radial displacement appears to be superimposed on a line which runs at a small angle to the undeformed (horizontal) orientation. The axial displacement is superimposed to one side of the undeformed location. As with the lower modes, the localized distortions at the shell ends is causing the radial displacement to have the appearance of  $m=6$ , while the axial displacement has the "mathematically correct"  $m=5$ , which corresponds to this being the fifth mode by order of frequency. The sixth mode at 874 Hz is also unusual. Now the radial displacement is superimposed to one side, and has the appearance of  $m=5$ . The correct interpretation is probably that  $m=6$ , as shown in the axial displacement and by order of frequency. It is interesting to note that these distorted modes have occurred at frequencies close to the extensional frequency of a ring (the frequency parameter  $\omega_0$ ). The seventh mode at 915 Hz has seven radial half waves, which corresponds to the ordering, but now the axial displacement has six waves. It seems probable that the axial displacements are now being distorted by the end conditions, causing them to appear to have a different number of half waves. This conclusion is reinforced by the similarity between this mode and the  $m=7$  (915 Hz) mode from the radial restraint case (Fig. 4.6). Comparison to the radial restraint case also aids in the interpretation of the remaining modes. If the two cases are compared, the ordering of the modes is the same, and the frequencies are similar. This leads to the conclusion that the 917 Hz mode of Fig. 4.11 is a superimposed version of the  $m=1$  mode from other frequency for this mode shape. (It was pointed out earlier that every mode shape has two distinct frequencies associated with it.)



Like the first  $m=1$  mode for these end conditions, the axial and radial displacements are shifted  $90^\circ$  and have localized distortions. In this mode, the axial displacement also has seven half waves superimposed on it, while the radial displacement has six. Due to the fact that this mode and the  $m=7$  mode are very close in frequency, it seems plausible that the mode shapes are combinations of these two modes. A similar superimposed shape is present in the second  $m=2$  mode at 1413 Hz, and can be explained in the same way.

The addition of axial restraint thus has a strong influence on the mode shapes. The identification of modes becomes very complicated due to differences between the mathematical number of half waves and the number visible in the displacement components. Further complications arise due to occasional superimposing of mode shapes with the mode shapes of nearby frequencies. Consideration of these effects, as well as the results from a similar case without axial restraint, help to properly interpret the mode shapes.

The effect of rotational restraint was investigated by adding the boundary condition  $\partial w / \partial x = 0$  to the previous case. The results are presented in Fig. 4.12, and should be compared to Fig. 4.11. The rotational restraint had a slight ( $<1\%$ ) effect on the lower modal frequencies, but its influence increased to over 5% at the highest modes reported. This is due to the increasing influence of the bending stiffness as the axial wave length decreases. This resulted in the frequency order of the modes being changed slightly. The mode that was established as  $m=5$  in the previous case now occurs at a higher frequency than the  $m=6$  mode, and the  $m=7$  mode is now higher than the second  $m=1$  mode.



\* Mode shape not illustrated

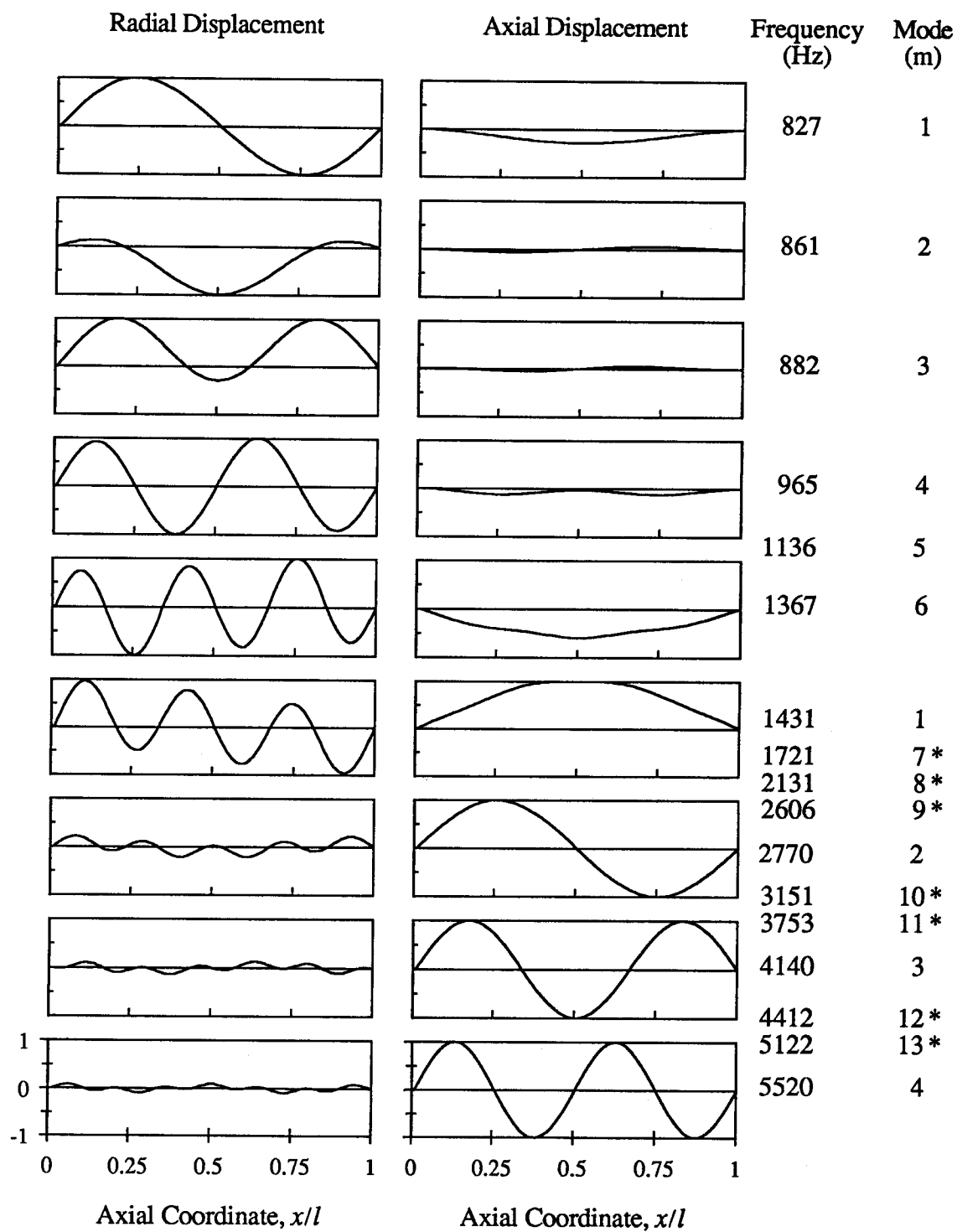
Fig. 4.12. Mode shapes with  $l/a=4$ ,  $a/h=20$  (end conditions  $u=w=\partial w/\partial x=0$ ).

Given that the axial restraint was shown to have the greatest influence on mode shapes, it is appropriate to look at how this effect might change with different  $l/a$  ratios. Figure 4.13 contains the results for  $l/a=2$ . Because this shell is shorter, the second and third modes are close to the ring frequency and show the superimposed effect. The second mode shapes for  $m=1, 2$ , and  $3$  have the shapes of nearby modes superimposed on the radial displacement. Figure 4.14 shows the results for  $l/a=8$ . Note that in this case there are many modes that occur below the ring frequency, so the superimposed mode shapes do not occur until the twelfth mode.

Figure 4.15 is a plot of the frequency spectrum containing the results from restraint conditions of  $w=0$  and  $u=w=0$ . This shows that in spite of the significant changes in mode shapes, the axial restraint had almost no effect on frequency. A strange effect was noted on the lower frequency curve in the region  $0.8 < l/ma < 2.0$ . In this region it appears as though the axial restraint caused a slight upward shift of the frequencies, toward the ring frequency. However, it is possible that this is due to numerical errors as the shift is on the order of 1%.

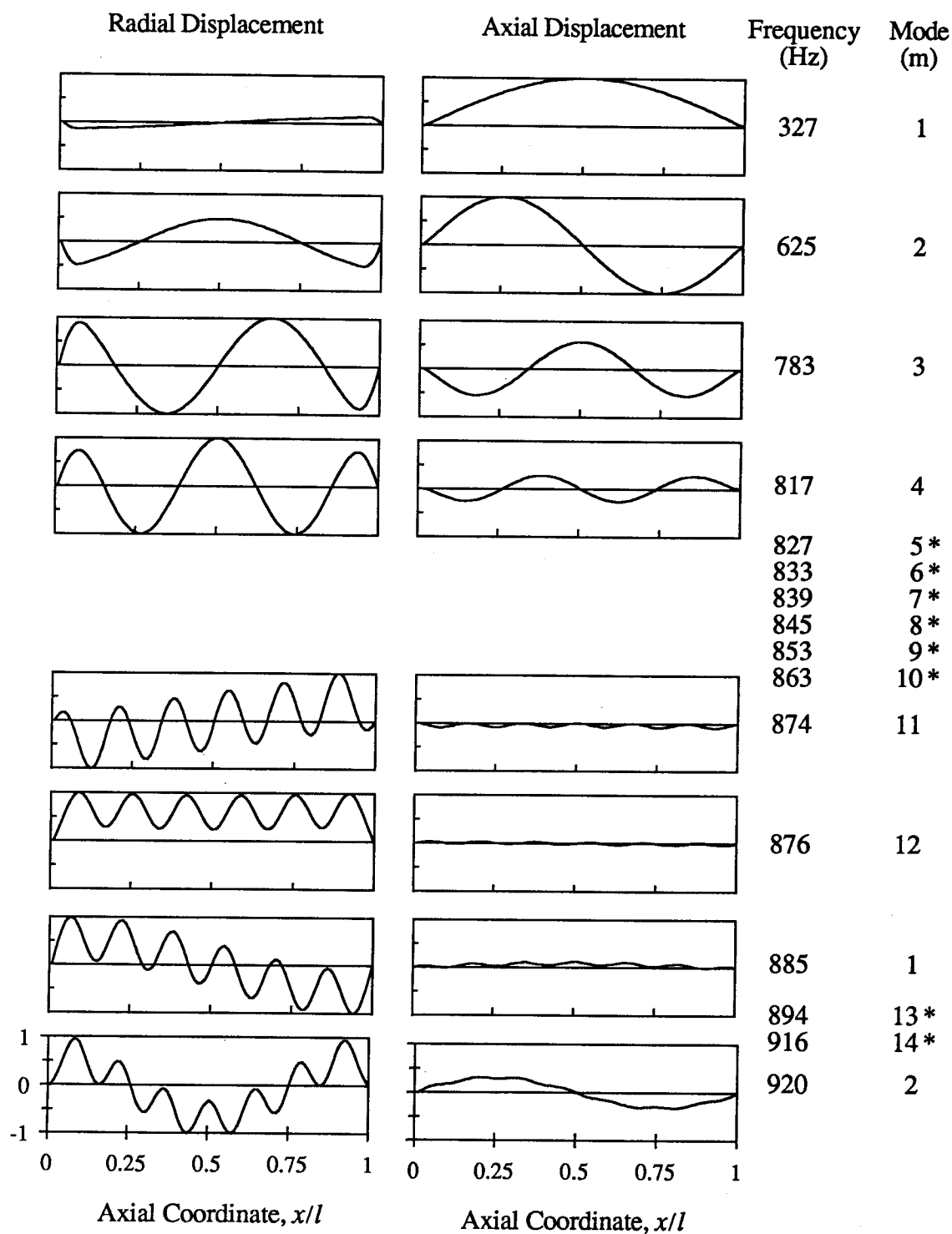
#### 4.6 References

- [4.1] ANSYS Engineering Analysis System User's Manual, Vol. I, Rev. 4.4, 1989.
- [4.2] Vronay, D. F. and Smith, B. L., "Free Vibrations of Circular Cylindrical Shells of Finite Length," *American Institute of Aeronautics and Astronautics Journal*, Vol. 8, No. 3, March 1970, pp. 601-603.
- [4.3] Goldman, R. L., "Mode Shapes and Frequencies of Clamped-Clamped Cylindrical Shells," *American Institute of Aeronautics and Astronautics Journal*, Vol. 12, No. 12, Dec. 1974, pp. 1755-1756.
- [4.4] Forsberg, K., "Axisymmetric and Beam-Type Vibrations of Thin Cylindrical Shells," *American Institute of Aeronautics and Astronautics Journal*, Vol. 7, No. 2, Feb. 1969, pp. 221-227.



\* Mode shape not illustrated

Fig. 4.13. Mode shapes with  $l/a=2$ ,  $a/h=20$  (end conditions  $u=w=0$ ).



\* Mode shape not illustrated

Fig. 4.14. Mode shapes with  $l/a=8$ ,  $a/h=20$  (end conditions  $u=w=0$ ).

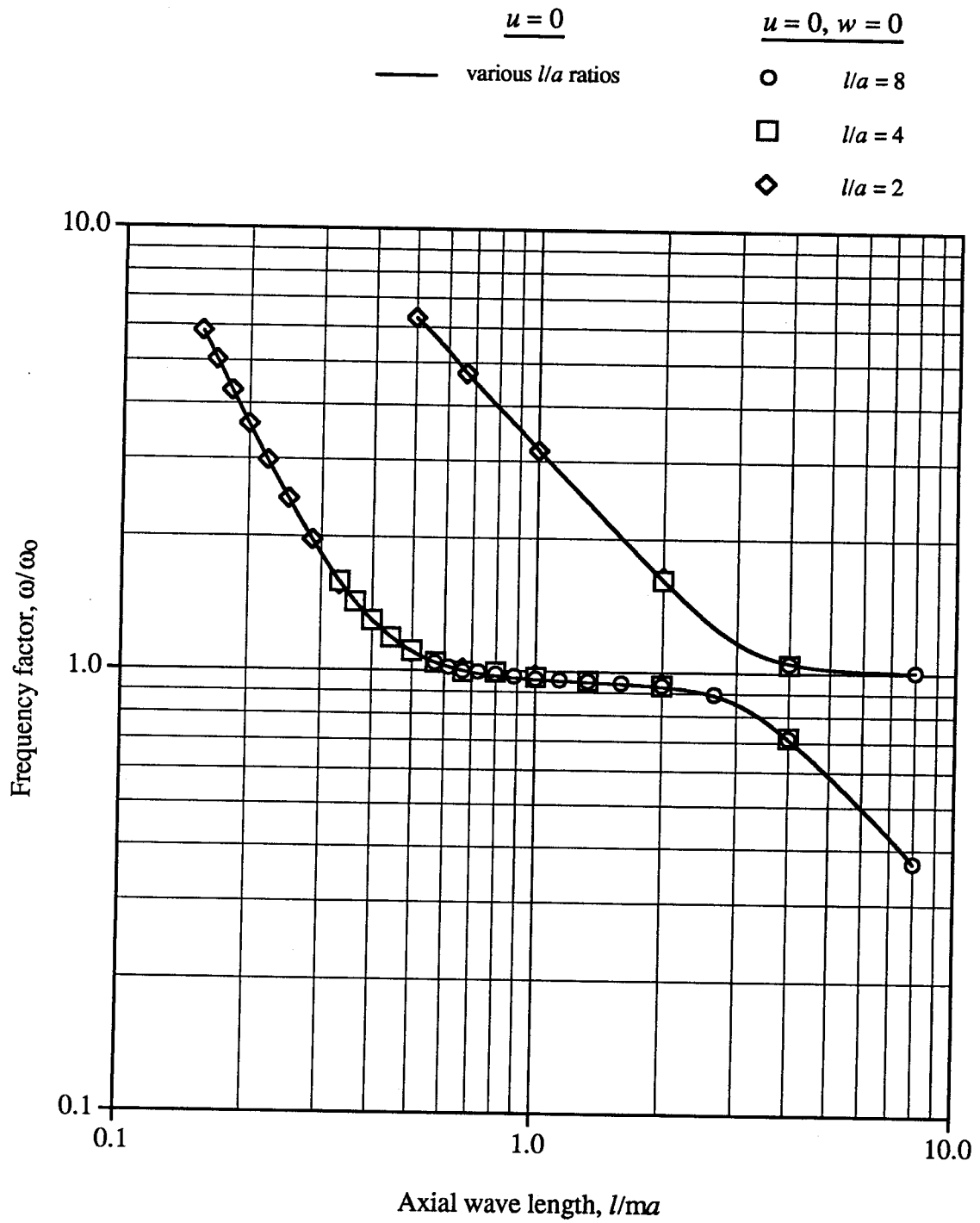


Fig. 4.15. Effect of axial restraint on frequency spectrum.

## Chapter 5

### Experimental Modal Analysis

In Chapter 4, finite element models were used to investigate the effect of end conditions on axisymmetric cylinder vibrations. It was found that cylinders of short to medium length may have very unusual mode shapes. This type of behavior is unusual for a linear structure, so an experimental investigation was carried out to verify these results.

#### 5.1 Experimental Setup

The purpose of the experimental phase of this investigation was to confirm the existence of the superimposed axisymmetric mode shapes that occurred under axial restraint in the finite element analysis. Previous investigators have found that perfectly clamped conditions are difficult to enforce in practice. However, Resnick [5.1] has shown that large end masses provide enough inertial resistance to approximate an axial restraint in cylinder modal analysis. Finite element models were used to determine the end mass necessary to simulate axial restraint and cause the superimposed modes to appear.

The sine excitation method was used to determine the modal frequencies and shapes. This technique is well documented; a comprehensive summary can be found in Ref. [5.2]. The method is based on the premise that if a sinusoidal excitation is applied to a linear system, the response will be sinusoidal. Furthermore, the amplitude ratio of the response to the excitation will be greatly increased when the frequency of the excitation is near a natural frequency of the system. This method

was the most widely used technique to carry out experimental modal analysis until the emergence of impulse testing in the last few decades. While the impulse method is generally faster and less tedious, the equipment available was not suitable for the high frequencies of the test cylinder.

The equipment used in the experiment is listed in Table 5.1. Excitation from the shaker was transmitted by a small rod threaded into the cylinder, which was supported by foam for isolation. The input force was measured by the load cell between the shaker and the rod. The accelerometer was attached using wax to allow easy movement between measurement locations. A digital frequency counter was used to monitor the input frequency, while the digital oscilloscope was used to compare the input and response for mode shape identification. Figure 5.1 is a schematic of the experimental setup, while Fig. 5.2 is a photograph of the actual system.

Table 5.1. List of experimental equipment.

Two Channel Digital Oscilloscope, Nicolet Model 3091
Frequency Counter-Timer, Fluke Model 1953A
Function Generator, Wavetek Model 110
Vibration Exciter, Brüel & Kjær Model 4809
Power Amplifier (for shaker), Brüel & Kjær Model 2706
Load Cell, PCB Model 208A02
Accelerometer, PCB Model 303A03
Power Supply, PCB Model 480B

The cylinder used in testing was cold drawn aluminum tubing with a nominal radius of 0.1046 m, thickness of 8.4 mm, and length of 0.260 m. These dimensions yield a radius to thickness ratio of 12.5 and a length to radius ratio of 2.5. Small holes were drilled at a quarter and half way from the ends to provide attachments for



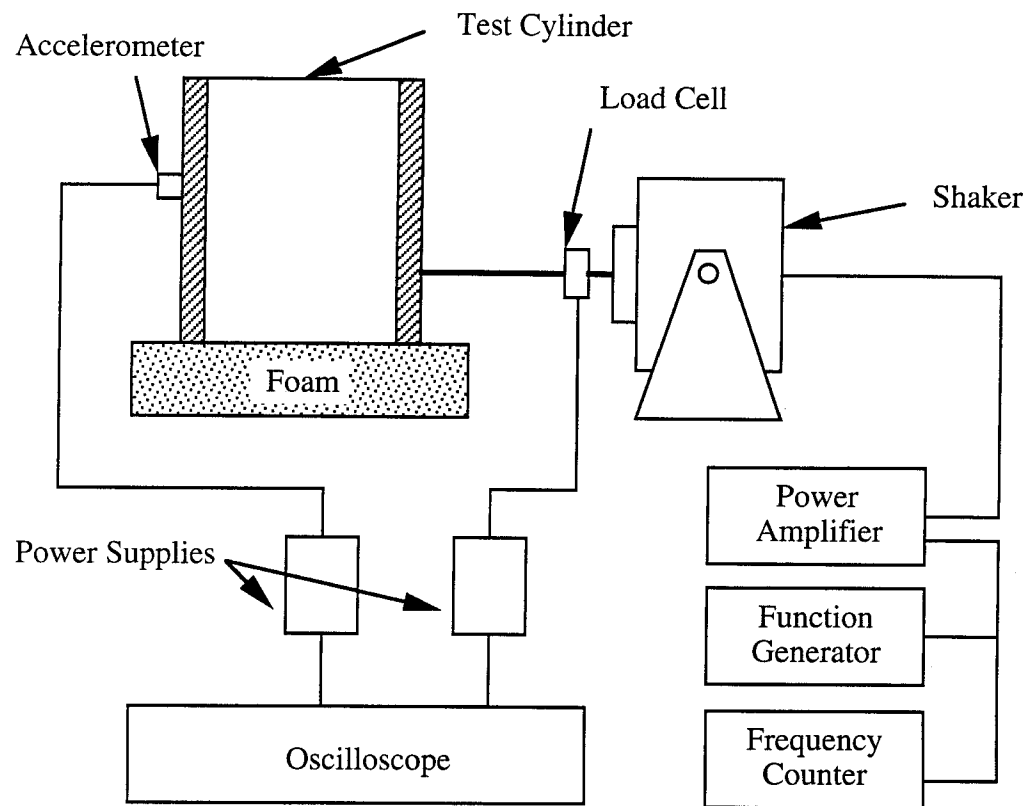


Fig. 5.1. Schematic of experimental modal analysis setup.

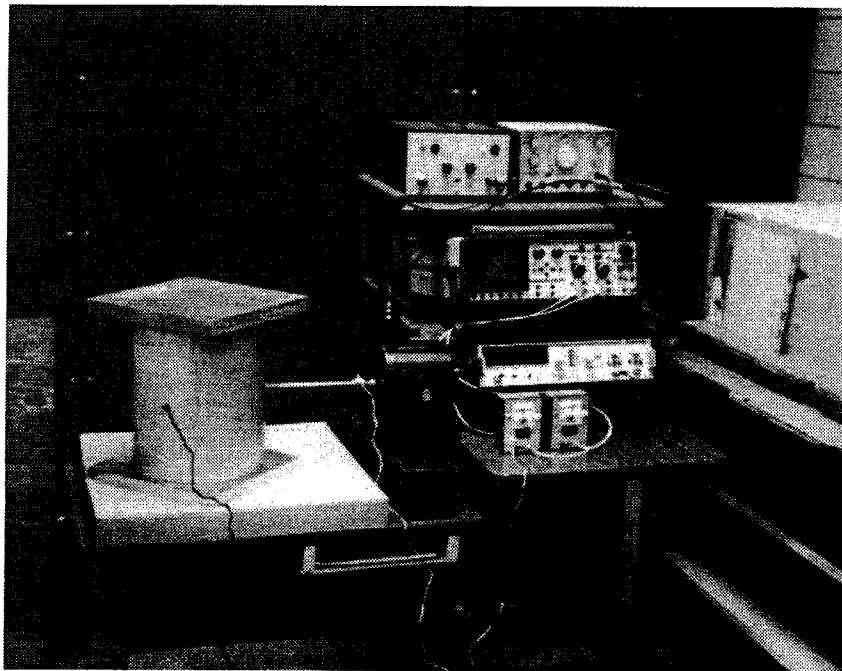


Fig. 5.2. Photo of experimental modal analysis setup.

the shaker. The different excitation points were used to excite the modes with large displacements at those locations. A grid was laid out on the outside surface of the cylinder to locate the measurement locations for initial mode identification. The grid lines were placed  $30^\circ$  apart in the circumferential direction and at five, equally-spaced locations along the length. The cylinder was tested initially in the free condition to verify the technique (results are presented in Section 5.3). Then to provide radial and axial restraint at the ends,  $0.25\text{ m} \times 0.25\text{ m} \times 0.025\text{ m}$  aluminum plates were bonded to the cylinder using cyanoacrylate adhesive (epoxy was also tried and found to be ineffective). Welding the end plates would have provided a more solid attachment, but was avoided due to concerns about weld non-uniformity and residual stresses causing distortion of the mode shapes.

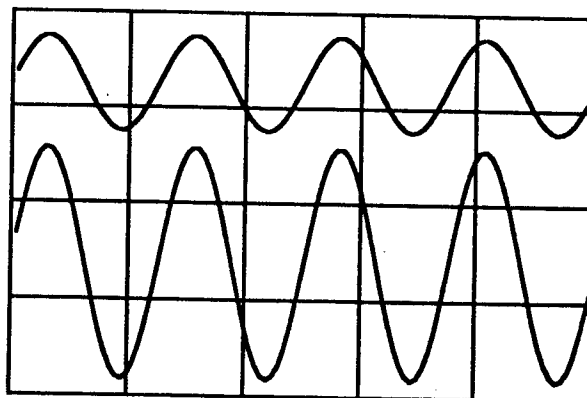
## 5.2 Experimental Procedure

A structure is said to have a resonance when an input force at a given frequency results in a very large amplitude response. Resonant frequencies were identified by observing the input and response while sweeping the excitation through frequencies of interest. Once the resonant frequencies were found, the associated mode shapes were identified by comparing the amplitude ratio and phase at various locations on the cylinder. Normally in vibrations testing, the accelerometer must be firmly attached to the surface of interest. In this case, due to the high frequency and low amplitude of the response, there was little difference between measurements whether the accelerometer was mounted using a stud, adhesive, wax, or merely held in place with a finger. Thus the modes could usually be identified by holding the accelerometer in place with a finger and sliding it along the surface in the

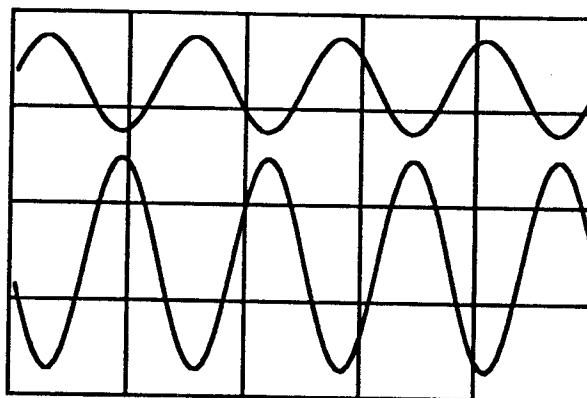
circumferential and axial directions. The accelerometer was mounted using wax when more accuracy was desired, e.g., when producing the mode shape plots.

In this study, only the axisymmetric modes were of interest. Hereafter, all the results presented in this chapter can be assumed to be for axisymmetric ( $n=0$ ) vibration.

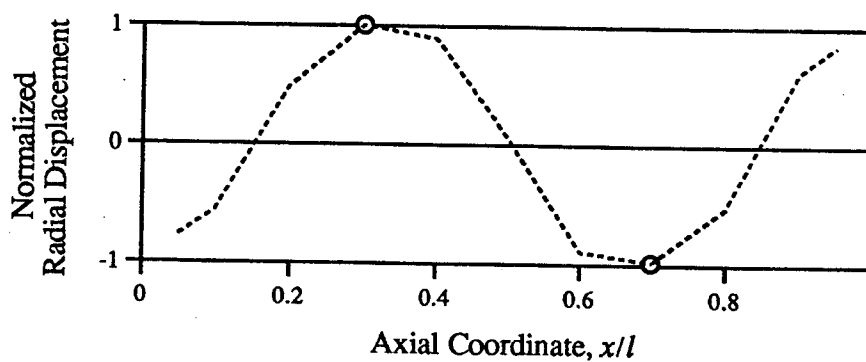
The mode shapes can be identified and plotted using the response-to-input amplitude ratio and phase information. The modal displacement is directly proportional to the amplitude ratio, and will be positive or negative depending on whether the response and excitation are in or out of phase. To illustrate this, representations of the measurements as seen on the oscilloscope are reproduced in Fig. 5.3. The traces correspond to the results obtained from the free cylinder while exciting at 8025 Hz. Figure 5.3a represents a measurement at one quarter of the way from one end, while Fig. 5.3b is at three quarters from the same end. In both plots the input force is the top trace, while the acceleration is the bottom trace. From Fig. 5.3a, the peak to peak amplitude of the response can be divided by that of the input, yielding an amplitude ratio of 2.4 between the signals at this location. The signals are in phase, which will arbitrarily be taken as a positive modal displacement. From Fig. 5.3b, this method yields an amplitude ratio of 2.2. At this location the signals are out of phase, which then corresponds to a negative modal displacement. These modal displacements can then be plotted as shown by the two data points in Fig. 5.3c. As more measurements are taken along the length of the cylinder, the mode shape plot can be filled in as indicated by the dotted line, in this case illustrating a mode with two axial half waves. The maximum modal displacements were normalized to unity as in the previous chapter.



(a) Input and response vs. time, measurement at  $x/l=0.25$



(b) Input and response vs. time, measurement at  $x/l=0.75$



(c) Mode shape plot

Fig. 5.3. Representation of experimental measurements and corresponding mode plot.

### 5.3 Experimental Results for Free Conditions

The modal analysis of the cylinder described in Section 5.1 was first carried out in the free state to verify the experimental procedure. Table 5.2 lists the frequencies obtained experimentally, the finite element frequencies, and the percent difference between them. The results show excellent correlation, as the frequencies are within a few percent. The plots in Fig. 5.4 compare the experimental mode shapes with those obtained using finite elements. The mode shapes show some fluctuations; possible sources of experimental error are imperfections in the cylinder and drifting of the excitation frequency. The amplitude ratio changes rapidly when the excitation approaches resonance, so the few Hertz variation noticed in the excitation frequency during measurements makes this suspect. The first, third, and fifth modes were obtained by applying the excitation at mid-span, while the second and fourth modes were excited at  $x/l=0.25$ .

Table 5.2. Comparison of experimental and finite element results with free end conditions ( $n=0$ ).

Mode Shape (# axial half waves)	Frequency (Hz)		Percent
	Experimental	Finite Elements	Difference
1	7402	7339	0.9
2	7822	7700	1.6
3	7868	7743	1.6
4	8025	7907	1.5
5	8597	8493	1.2

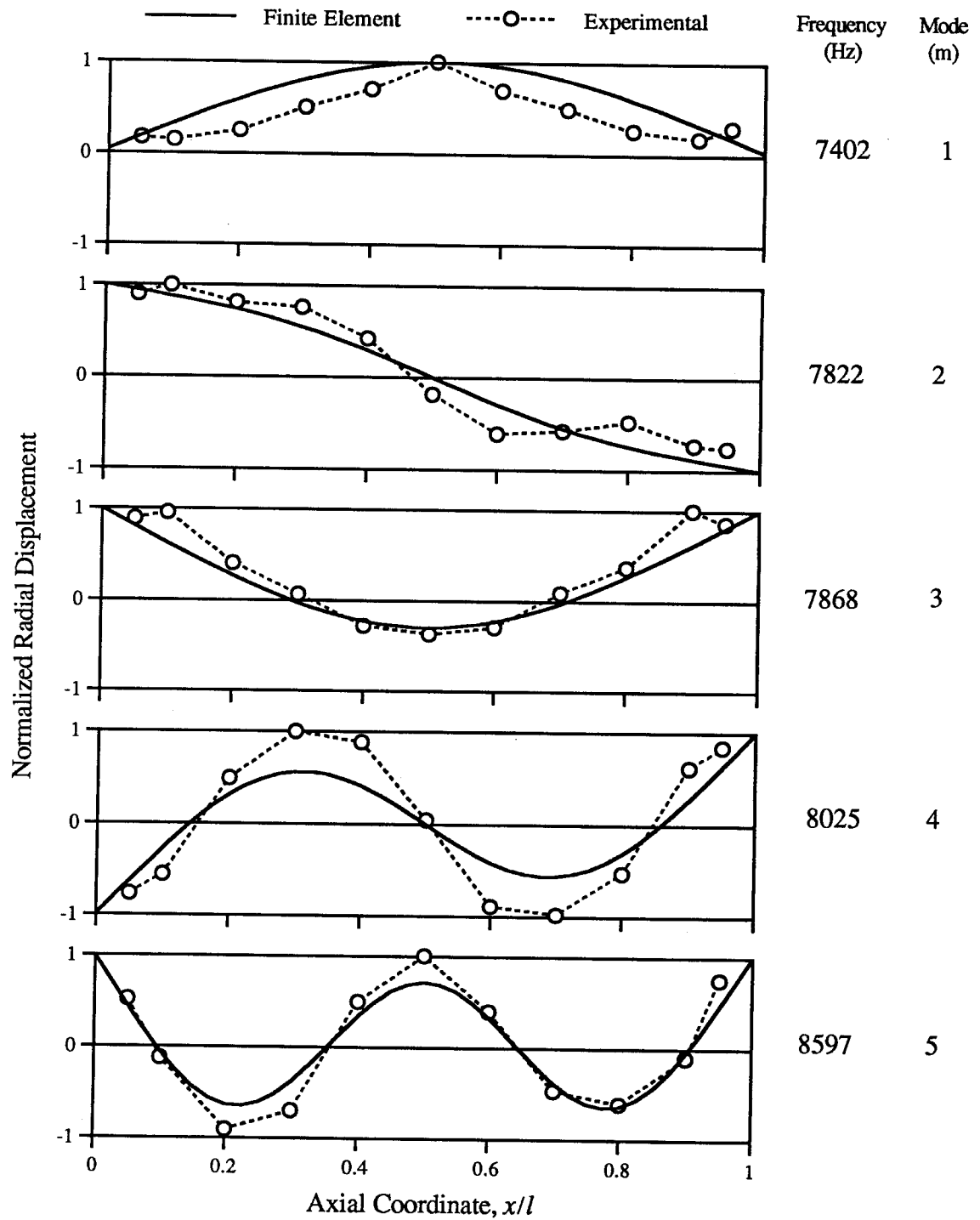


Fig. 5.4. Mode shapes with free end conditions, showing experimental and finite element results.

#### 5.4 Experimental Results with End Plates

Once the experimental technique had been verified, the end plates were bonded onto the ends of the cylinder (dimensions given in Section 5.1) and the tests were repeated. Although the end plates are actually square, they were assumed to be round so that an axisymmetric finite element model could be used to predict the response. The outside diameter of the plates was taken as 0.25 m, which corresponds to the minimum diameter provided by the 0.25 m square plates. Due to the thickness of the end plates, 4-node elements were used rather than the 2-node shell elements.

Table 5.3 lists the experimental and finite element frequencies, and the percent difference between them. As before, the results compare extremely well. The plots in Fig. 5.5 show the experimental and finite element mode shapes in order of increasing frequency. The second mode was obtained by applying the excitation at mid-length, while the remaining modes were excited at  $x/l=0.25$ . The plots show excellent agreement between experiment and finite elements, and also clearly verify the existence of the superimposed mode shapes.

Table 5.3. Comparison of experimental and finite element results with clamped end conditions simulated by end plates ( $n=0$ ).

Mode Shape (# axial half waves)	Frequency (Hz)		Percent
	Experimental	Finite Elements	Difference
1	7801	7783	0.2
2	8171	8201	0.4
3	8503	8568	0.8
4	9398	9260	1.5

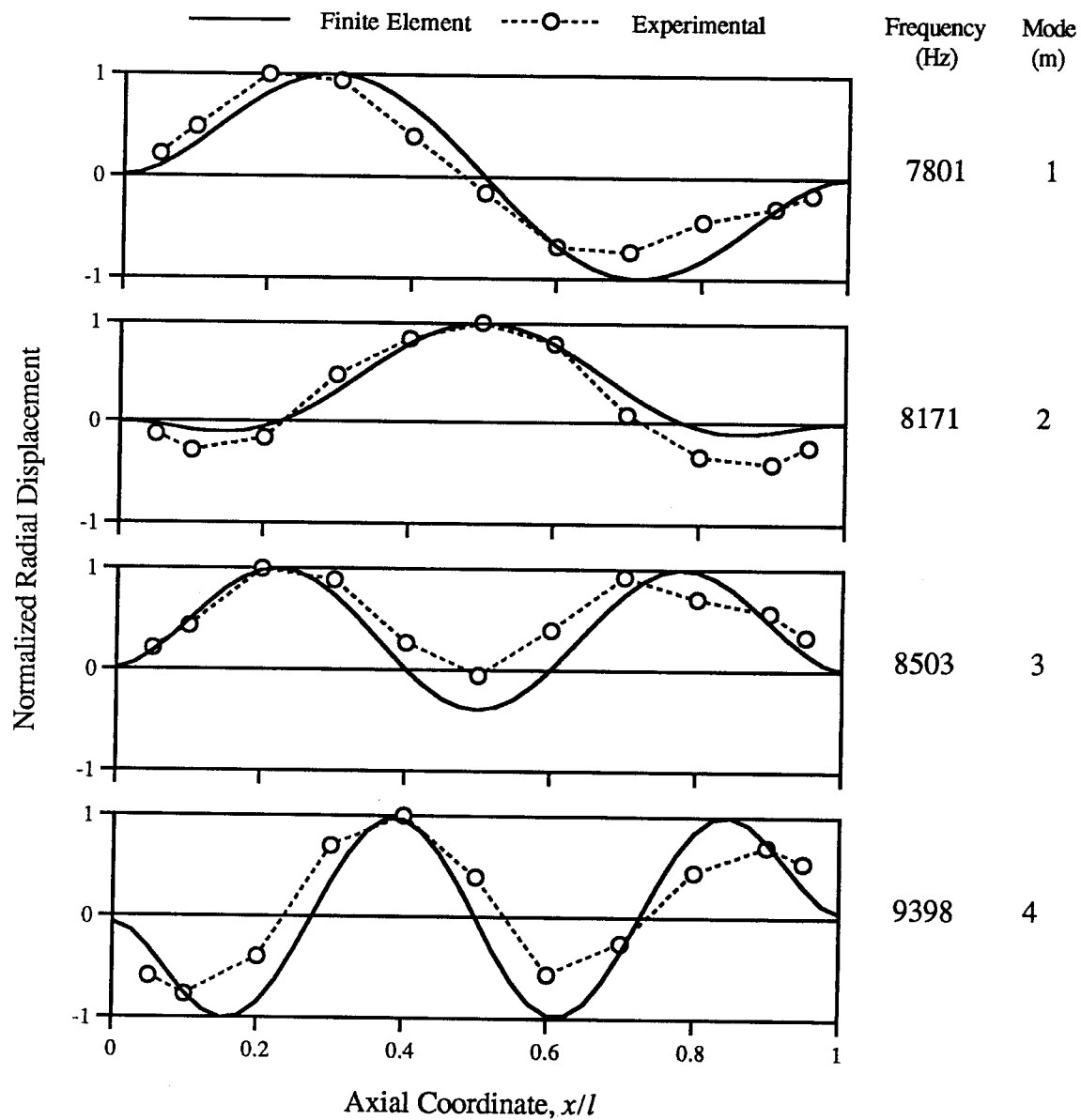


Fig. 5.5. Mode shapes with end plates, showing experimental and finite element results.



## 5.5 References

- [5.1] Resnick, B. S. and Dugundji, J., "The Effects of Orthotropicity and Reinforcements on the Vibrations of Cylindrical Shells," MIT Aeroelastic and Structures Research Lab Report ASRL-TR-134-2, November 1966.
- [5.2] Smith, J. D., *Vibration Measurement and Analysis*, Butterworths, Boston, 1989.

## Chapter 6

### Summary and Conclusions

The axisymmetric vibration characteristics of cylinders must be known in order to predict the response to internal blast loads. A review of analytical methods for predicting shell vibrations showed that the general equations of motion are very difficult to solve, even for the axisymmetric case. Neglecting tangential inertia helps simplify the equations of motion, but can lead to errors in predicting the natural frequencies and mode shapes when the wavelength parameter  $l/ma$  is between 0.5 and 10. The resulting equations also do not predict the superimposed mode shapes noted in this study.

Finite element models were developed to further investigate the effect of cylinder dimensions and end conditions on the modal characteristics. This was found to be a very effective analysis method.

It was noted by previous researchers that the natural frequencies change only slightly when various symmetric end conditions are applied. This was found to be generally true in this study. However, it was noted that the boundary conditions had a noticeable effect on the frequency (up to 5%) when the cylinder was relatively thick ( $a/h > 20$ ), as might be expected. While the end conditions did not have large effects on the modal frequencies, they had a much greater effect on the mode shapes.

Previous researchers have stated that the case of free end conditions produces the same results as that of radial restraint. However, it was found that the mode shapes only matched for the lowest modes. For higher modes the shapes were significantly different. In addition, the frequencies for free end conditions were lower by a few

percent in the higher modes. Another interesting phenomenon was that the modal frequencies that were just below  $\omega_o$  (the primary extensional frequency of a ring with the same properties) increased toward  $\omega_o$  slightly.

The effect of rotational restraint was also investigated. The rotational restraint had a slight (<1%) effect on the lower modal frequencies, but its influence increased to over 5% at the highest modes reported. This is due to the increasing influence of the bending stiffness as the axial wave length decreases. It can result in the frequency ordering of the modes being changed slightly.

The addition of axial restraint was found to have a strong influence on the mode shapes. The identification of modes becomes very complicated due to differences between the mathematical number of half waves and the number visible in the displacement components. Further complications arise due to occasional superimposing of mode shapes with the mode shapes of nearby frequencies. Consideration of these effects, as well as the results from a similar case without axial restraint, help to properly interpret the mode shapes. The use of incorrect modal characteristics in predicting the transient response can lead to serious errors. Therefore, these results are an important first step toward accurate assessment of internal blast loadings on cylinders.